

Superdirective Antenna Pairs for Energy-Efficient Terahertz Massive MIMO

Konstantinos Dovelos, *Graduate Student Member, IEEE*, Stylianos D. Assimonis, Hien Quoc Ngo, *Senior Member, IEEE*, and Michail Matthaiou, *Senior Member, IEEE*

Abstract

Terahertz (THz) communication is widely deemed the next frontier of wireless networks owing to the abundant spectrum resources in the THz band. Whilst THz signals suffer from severe propagation losses, a massive antenna array can be deployed at the base station (BS) to mitigate those losses through beamforming. Nevertheless, a large number of antennas increases the hardware complexity and circuit power consumption, and hence it can lead to poor energy efficiency (EE). To surmount this fundamental problem, we propose a novel array design based on coupled antenna pairs. Specifically, we exploit the mutual coupling between closely spaced antennas to form superdirective pairs. A unique property of them is that all require the same excitation amplitude, and therefore can be driven by a single radio frequency chain akin to conventional phased arrays. Moreover, they facilitate the implementation of multi-port impedance matching, which ensures maximum power transfer for any beamforming angle. After addressing the hardware-related problems of superdirectivity, we show that the number of BS antennas can be effectively reduced without sacrificing the achievable rate. Simulation results showcase that our design offers huge EE gains compared to uncoupled uniform linear arrays, and hence could be a radical solution for future THz systems.

Index Terms

Antenna arrays, channel estimation, energy efficiency, hybrid beamforming, impedance matching, mutual coupling, superdirectivity, THz communications.

I. INTRODUCTION

Massive multiple-input multiple-output (MIMO) is now a mature technology, which has been adopted by 5G new radio to provide superior network capacity and coverage [1]. In parallel, millimeter wave (mmWave) systems start gaining ground as an effective way for delivering multi-gigabit rates thanks to their very large bandwidths [2], [3]. Toward this direction, communication above 100 GHz, i.e., terahertz (THz) frequencies, is widely deemed the next frontier of wireless systems with a plethora of promising

All authors are with the Centre for Wireless Innovation (CWI), Queen's University Belfast, Belfast BT3 9DT, U.K., email: {k.dovelos, s.assimonis, hien.ngo, m.matthaiou}@qub.ac.uk.

applications, ranging from ultra-broadband femtocells to terabit-per-second links for wireless backhaul [4]. Nevertheless, THz signals are subject to severe propagation and molecular absorption losses, which can drastically limit the communication range and coverage [5]. To deal with this problem, large antenna arrays can be deployed at the BS to increase the signal power by means of sharp beamforming. As a result, massive MIMO is expected to be an integral component of future THz systems [6], [7]. On the other hand, THz radio frequency (RF) circuits, e.g., power amplifiers, phase shifters, etc., exhibit significantly higher power consumption than their sub-6 GHz counterparts [8]. Additionally, multi-dimensional signal processing during channel estimation and data transmission is power intensive [9]. In conclusion, achieving a large beamforming gain in an energy efficient manner constitutes a major engineering challenge which calls for novel solutions.

The beamforming capabilities of multi-antenna systems have been extensively investigated in the past. For example, a typical N -element phased array offers a gain that scales linearly with N when maximum ratio transmission (MRT) is used [10]. However, higher gains are possible by leveraging the mutual coupling between adjacent antennas. Specifically, Uzkov theoretically proved in his seminal work [11] that a uniform linear array (ULA) of N isotropic radiators and vanishingly small inter-element spacing has an endfire directivity of N^2 , a phenomenon now known as *superdirectivity*.

The theme of superdirectivity has been studied from both information theoretic and pure electromagnetic standpoints, e.g., [12]–[17], and references therein. However, most of the related literature considers arrays of uniform spacing. More importantly, it overlooks various communication and practical aspects, such as EE, implementation limitations in hybrid analog-digital architectures, and channel estimation performance. Consequently, there are still critical questions about how THz massive MIMO could fully benefit from superdirectivity. Regarding other approaches, there is a stream of recent papers on arrays-of-subarrays (AoSA) [18]–[20] and intelligent reflecting surfaces [21], which can improve the EE. Yet, they neglect mutual coupling and assume a uniformly-spaced antenna array at the BS.

This paper aims to show that superdirectivity can be ingeniously used to reduce the hardware complexity and boost the EE of THz massive MIMO. The contributions of our work are summarized as follows:

- We introduce a coupling-aware array model based on *antenna theory*. In particular, we derive the input impedance matrix of the BS array assuming lossy dipole antennas. Note that directive antennas, such as linear dipoles, are mutually coupled even for half-wavelength spacing. Therefore, proper characterization of their electromagnetic interaction is crucial to beamforming [22].

- Based on the introduced array model, we study the implementation issues of superdirectivity. In particular, we look into the impedance matching problem as well as the realization of superdirective beamsteering in a hybrid analog-digital array architecture. We address both problems by proposing a novel array design relying on coupled antenna pairs. Specifically, the BS array is divided into multiple two-element groups, which are adequately separated so that inter-group coupling can be neglected. The resulting nonuniform linear array (NULA) greatly simplifies optimal multi-port matching, and more importantly, requires uniform amplitude excitation. Consequently, it can be driven by a single RF chain to produce a pencil-like beam, similar to conventional phased arrays. It is worth stressing that our method can be readily applied to an AoSA, wherein each subarray is a NULA.
- We exploit the excessive power gain of the proposed NULA to decrease the number of BS antennas. This leads to a low-dimensional massive MIMO system, whose performance is assessed in terms of the achievable rate under perfect and imperfect channel state information (CSI). For this purpose, approximate closed-form expressions for the signal and interference powers are provided assuming MRT. Moreover, the channel estimation problem is addressed by leveraging the popular orthogonal matching pursuit (OMP) algorithm.
- Extensive simulation results are provided corroborating our analysis. In particular, it is demonstrated that the proposed array design boosts the EE of THz massive MIMO without sacrificing the data transmission and channel estimation performances. As such, it has the potential to realize low-complexity, energy-efficient, and compact MIMO arrays with sharp beamforming capabilities.

The rest of the paper is organized as follows: Section II delineates the BS array model. Section III presents the impedance matching problem. Section IV concerns the implementation issues of superdirectivity and details the proposed solution. Section V introduces the system model used in performance evaluation. Section VII addresses the channel estimation problem. Section IX is devoted to numerical simulations. Finally, Section X summarizes the main conclusions of this work.

Notation: Throughout the paper, $D_N(x) = \frac{\sin(Nx/2)}{N \sin(x/2)}$ is the Dirichlet sinc function; $\mathbf{A}(\cdot, \cdot, \cdot)$ is a vector field; \mathbf{A} is a matrix; \mathbf{A}^* , \mathbf{A}^\dagger , \mathbf{A}^H , and \mathbf{A}^T are the conjugate, pseudoinverse, conjugate transpose, and transpose of \mathbf{A} , respectively; $[\mathbf{A}]_{i,j}$ is the (i, j) th entry of \mathbf{A} ; $\mathbf{A}(i)$ is the i th column of \mathbf{A} ; $\text{blkdiag}(\mathbf{A}_1, \dots, \mathbf{A}_n)$ is a block diagonal matrix; \mathbf{a} is a vector; $\|\mathbf{a}\|_1$ and $\|\mathbf{a}\|$ are the l_1 -norm and l_2 -norm of \mathbf{a} , respectively; $\text{mag}(\mathbf{a}) = [|a_1|, \dots, |a_N|]^T$ for $\mathbf{a} = [a_1, \dots, a_N]^T$; $\mathbf{1}_{N \times M}$ is the $N \times M$ matrix with unit entries; \mathbf{I}_N is the $N \times N$ identity matrix; $\mathbf{0}_{N \times M}$ is the $N \times M$ matrix with zero entries; \otimes denotes the Kronecker product;

$\mathbf{a} \cdot \mathbf{b}$ is the inner product between \mathbf{a} and \mathbf{b} ; $\mathbb{E}\{\cdot\}$ denotes expectation; $\mathcal{CN}(\boldsymbol{\mu}, \mathbf{R})$ is a complex Gaussian vector with mean $\boldsymbol{\mu}$ and covariance matrix \mathbf{R} ; while $\text{Re}\{\cdot\}$ and $\text{Im}\{\cdot\}$ are the real and imaginary parts of a complex variable, respectively.

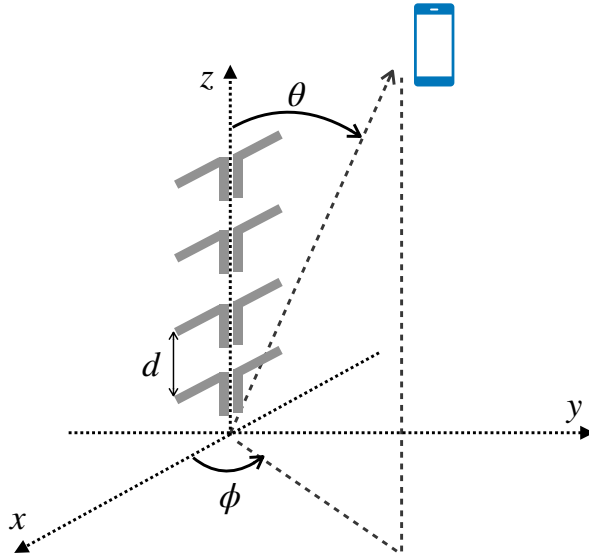


Fig. 1: Illustration of the ULA geometry considered in the array model.

TABLE I
MAIN NOTATION IN THE ARRAY MODEL

Notation	Description
N	Number of BS antennas
d	Inter-element spacing
f	Carrier frequency
λ	Carrier wavelength
κ	Wavenumber
ℓ	Dipole length
ρ	Dipole radius
η	Impedance of free-space
μ	Permeability of free-space
σ_c	Copper conductivity
$\mathbf{Z}_{\text{ideal}}$	Input impedance matrix for lossless dipoles
\mathbf{Z}	Input impedance matrix for lossy dipoles

II. ANTENNA ARRAY MODEL

In this section, we present the BS array model which takes into account antenna mutual coupling.

A. Radiated Power

Consider an N -element ULA along the z -axis at the BS, as depicted in Fig. 1. The inter-element spacing is d . Each element is a linear dipole parallel to the x -axis, and is of length ℓ and radius ρ . According

to [23, Ch. 4], the current distribution on each dipole n has approximately the sinusoidal form

$$I_n(x') \approx I_n(0) \frac{\sin(\kappa\ell/2 - \kappa|x'|)}{\sin(\kappa\ell/2)}, \quad |x'| \leq \ell/2, \quad (1)$$

where $I_n(0) \in \mathbb{C}$ is the input current, $\kappa = 2\pi/\lambda$ is the wavenumber, and λ is the wavelength. We next focus on an arbitrary user who is in the far field of the BS array. The user's location is described by the tuple $(r \cos \phi \sin \theta, r \sin \phi \sin \theta, r \cos \theta)$, where $r, \theta \in [0, \pi]$, and $\phi \in [0, 2\pi]$ are the radial distance, polar angle, and azimuth angle, respectively. The electric field at the user is then specified as (see Appendix A)

$$\mathbf{E}(r, \theta, \phi) = -j\eta \frac{e^{-j\kappa r}}{2\pi r} \sum_{n=0}^{N-1} e^{j\kappa \hat{\mathbf{r}} \cdot \mathbf{r}_n} I_n(0) \mathbf{F}(\theta, \phi), \quad (2)$$

where

$$\mathbf{F}(\theta, \phi) = \frac{\cos(\kappa\ell/2 \cos \phi \sin \theta) - \cos(\kappa\ell/2)}{\sin(\kappa\ell/2)(\sin^2 \phi + \cos^2 \phi \cos^2 \theta)} (\cos \theta \cos \phi \mathbf{e}_\theta - \sin \phi \mathbf{e}_\phi) \quad (3)$$

is the vector field pattern of each dipole, \mathbf{e}_θ and \mathbf{e}_ϕ are the unit vectors along the polar and azimuth directions, respectively, η is the characteristic impedance of free-space, $\hat{\mathbf{r}} = (\cos \phi \sin \theta, \sin \phi \sin \theta, \cos \theta)^T$ is the unit radial vector along the user direction, and $\mathbf{r}_n = (0, 0, nd)$ is the position vector of the n th antenna. The radiation intensity [W/sr] is written in vector form as

$$U \triangleq \frac{\|\mathbf{E}(r, \theta, \phi)\|^2}{2\eta} r^2 = \frac{\eta}{8\pi^2} \|\mathbf{F}(\theta, \phi)\|^2 |\mathbf{a}^H(\theta) \mathbf{i}|^2, \quad (4)$$

where $\mathbf{a}(\theta) = [e^{-j\kappa \hat{\mathbf{r}} \cdot \mathbf{r}_0}, \dots, e^{-j\kappa \hat{\mathbf{r}} \cdot \mathbf{r}_{N-1}}]^T \in \mathbb{C}^{N \times 1}$ and $\mathbf{i} = [I_0(0), \dots, I_{N-1}(0)]^T \in \mathbb{C}^{N \times 1}$ are the far-field array response vector and the vector of input currents, respectively. Using (4), the power radiated by the antenna array is

$$\begin{aligned} P_{\text{rad}} &= \int_0^\pi \int_0^{2\pi} U \sin \theta d\theta d\phi = \frac{1}{2} \mathbf{i}^H \underbrace{\left(\frac{\eta}{4\pi^2} \int_0^\pi \int_0^{2\pi} \mathbf{a}(\theta) \mathbf{a}^H(\theta) \|\mathbf{F}(\theta, \phi)\|^2 \sin \theta d\theta d\phi \right)}_{\text{Re}\{\mathbf{Z}_{\text{ideal}}\}} \mathbf{i} \\ &= \frac{1}{2} \mathbf{i}^H \text{Re}\{\mathbf{Z}_{\text{ideal}}\} \mathbf{i}, \end{aligned} \quad (5)$$

where $\mathbf{Z}_{\text{ideal}} \in \mathbb{C}^{N \times N}$ is the input impedance matrix of the array assuming *lossless* antennas. Moreover, $R_i \triangleq [\text{Re}\{\mathbf{Z}_{\text{ideal}}\}]_{n,n} = \frac{\eta}{4\pi^2} \int_0^\pi \int_0^{2\pi} \|\mathbf{F}(\theta, \phi)\|^2 \sin \theta d\theta d\phi$ is the input resistance¹ of each lossless dipole.

¹Recall that the input resistance equals the radiation resistance divided by $\sin(\kappa\ell/2)$ [23, Ch. 8]. This is because all quantities are expressed in terms of the input currents rather than the current maxima $\{I_n(0)/\sin(\kappa\ell/2)\}_{n=0}^{N-1}$.

B. Input Power and Array Gain

Realistic dipole antennas exhibit a conduction/loss resistance which leads to heat dissipation. Because of the *skin effect* of conductive wires carrying an alternating current, the loss resistance per unit length is given by [23, Eq. (2-90b)]

$$\bar{R}_{\text{loss}} = \frac{1}{2\rho} \sqrt{\frac{f\mu}{\pi\sigma_c}}, \quad (6)$$

where f is the carrier frequency, μ is the permeability of free-space, and σ_c is the conductivity of the wire material. Under the sinusoidal current distribution in (1), the loss resistance relative to the input current $I_n(0)$ is then specified as

$$R_{\text{loss}} = \bar{R}_{\text{loss}} \int_{-\ell/2}^{\ell/2} \left| \frac{I_n(x')}{I_n(0)} \right|^2 dx' = \frac{\kappa\ell - \sin(\kappa\ell)}{4\kappa\rho \sin^2\left(\frac{\kappa\ell}{2}\right)} \sqrt{\frac{f\mu}{\pi\sigma_c}}, \quad (7)$$

which yields the overall power loss [24]

$$P_{\text{loss}} = \frac{1}{2} \sum_{n=0}^{N-1} R_{\text{loss}} |I_n(0)|^2 = \frac{1}{2} R_{\text{loss}} \|\mathbf{i}\|^2. \quad (8)$$

Consequently, the input power at the antenna ports is

$$\begin{aligned} P_{\text{in}} &= P_{\text{loss}} + P_{\text{rad}} \\ &= \frac{1}{2} R_{\text{loss}} \|\mathbf{i}\|^2 + \frac{1}{2} \mathbf{i}^H \mathbf{Re}\{\mathbf{Z}_{\text{ideal}}\} \mathbf{i} = \frac{1}{2} \mathbf{i}^H \mathbf{Re}\{\mathbf{Z}\} \mathbf{i}, \end{aligned} \quad (9)$$

where $\mathbf{Z} \triangleq R_{\text{loss}} \mathbf{I}_N + \mathbf{Z}_{\text{ideal}}$ is the impedance matrix of the lossy array. Finally, the array gain is defined as

$$G(\theta, \phi) \triangleq \frac{4\pi U}{P_{\text{in}}} = G_e(\theta, \phi) (R_{\text{loss}} + R_i) \frac{|\mathbf{a}^H(\theta) \mathbf{i}|^2}{\mathbf{i}^H \mathbf{Re}\{\mathbf{Z}\} \mathbf{i}}, \quad (10)$$

where $G_e(\theta, \phi) = \frac{\eta \|\mathbf{F}(\theta, \phi)\|^2}{\pi(R_{\text{loss}} + R_i)}$ denotes the gain of each dipole.

C. Optimal Currents under Fixed Input Power

According to Friis transmission formula, the power received by the user is given by [23]

$$P_r = P_{\text{in}} \left(\frac{\lambda}{4\pi r} \right)^2 G(\theta, \phi), \quad (11)$$

where an isotropic antenna has been assumed at the user for simplicity. We now seek to find \mathbf{i} that maximizes the received power (or equivalently $G(\theta, \phi)$) subject to the input power constraint $P_{\text{in}} \leq P_t$. The

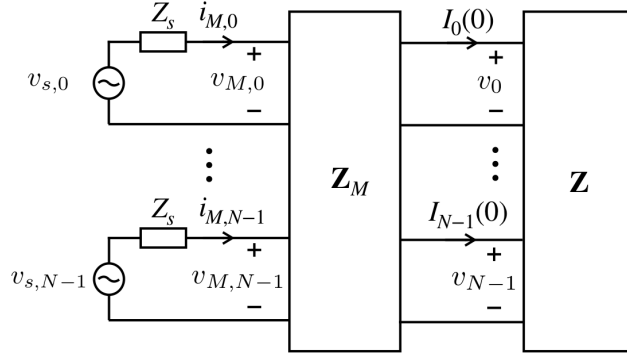


Fig. 2: Equivalent multi-port network of an antenna array covering signal generation, impedance matching, and antenna coupling.

objective (10) is a generalized Rayleigh quotient. Thus, the optimal current excitation is obtained as [24]

$$\mathbf{i}^* = \sqrt{\frac{2P_t}{\mathbf{a}^H(\theta)\text{Re}\{\mathbf{Z}\}^{-1}\mathbf{a}(\theta)}} \text{Re}\{\mathbf{Z}\}^{-1}\mathbf{a}(\theta), \quad (12)$$

and the maximum array gain is

$$G_{\max}(\theta, \phi) = G_e(\theta, \phi)(R_{\text{loss}} + R_i)\mathbf{a}^H(\theta)\text{Re}\{\mathbf{Z}\}^{-1}\mathbf{a}(\theta). \quad (13)$$

Remark 1 (Uncoupled ULA). *In the absence of mutual coupling, $\text{Re}\{\mathbf{Z}_{\text{ideal}}\} = R_i\mathbf{I}_N$ and $P_{\text{rad}} = \frac{1}{2}R_i\|\mathbf{i}\|^2$. Moreover, $\mathbf{i}^* = \sqrt{\frac{2P_t}{N(R_{\text{loss}}+R_i)}}\mathbf{a}(\theta)$ and $G_{\max}(\theta, \phi) = G_e(\theta, \phi)N$, which is the typical $O(N)$ power gain.*

III. IMPEDANCE MATCHING IN THE PRESENCE OF MUTUAL COUPLING

Mutual coupling alters the input impedance of each dipole. To see this, let $\mathbf{v} = [v_0, \dots, v_{N-1}]^T \in \mathbb{C}^{N \times 1}$ denote the vector of voltages at the antenna ports. Then, we have that $\mathbf{v} = \mathbf{Z}\mathbf{i} = \mathbf{Z}_a\mathbf{i}$, where $\mathbf{Z}_a \in \mathbb{C}^{N \times N}$ is a diagonal matrix with entries [23, Ch. 8]

$$[\mathbf{Z}_a]_{n,n} \triangleq \left([\mathbf{Z}]_{n,n} + \sum_{m=0, m \neq n}^{N-1} [\mathbf{Z}]_{n,m} \frac{I_m(0)}{I_n(0)} \right), \quad (14)$$

where $[\mathbf{Z}_a]_{n,n}$ is the *active* impedance of the n th antenna. The active impedance of each dipole hinges on the excitation currents, and hence single-port conjugate matching is optimal only for a specific beamforming angle θ [25]. For this reason, we resort to multi-port matching and model the BS array as in Fig. 2. The impedance network is a *lossless* $2N$ -port network described by the matrix $\mathbf{Z}_M \in \mathbb{C}^{2N \times 2N}$, which is partitioned as

$$\mathbf{Z}_M = \begin{bmatrix} \mathbf{Z}_{M11} & \mathbf{Z}_{M12} \\ \mathbf{Z}_{M21} & \mathbf{Z}_{M22} \end{bmatrix}. \quad (15)$$

The lossless property implies that \mathbf{Z}_M has only imaginary entries. The vector of voltage sources is denoted by $\mathbf{v}_s = [v_{s,0}, \dots, v_{s,N-1}]^T \in \mathbb{C}^{N \times 1}$. Each voltage source has an internal impedance $Z_s \in \mathbb{C}$, with $\text{Re}\{Z_s\} = R_s$. Likewise, the voltages and currents at the input ports of the network are denoted by $\mathbf{v}_M = [v_{M,0}, \dots, v_{M,N-1}]^T \in \mathbb{C}^{N \times 1}$ and $\mathbf{i}_M = [i_{M,0}, \dots, i_{M,N-1}]^T \in \mathbb{C}^{N \times 1}$, respectively. Based on basic circuit analysis, the relationship between the voltages and currents at the input and output of the matching network is [26]

$$\begin{bmatrix} \mathbf{v}_M \\ \mathbf{v} \end{bmatrix} = \begin{bmatrix} \mathbf{Z}_{M11} & \mathbf{Z}_{M12} \\ \mathbf{Z}_{M21} & \mathbf{Z}_{M22} \end{bmatrix} \begin{bmatrix} \mathbf{i}_M \\ -\mathbf{i} \end{bmatrix}. \quad (16)$$

Using (16) and the relationship $\mathbf{v} = \mathbf{Z}\mathbf{i}$ yields

$$\mathbf{v}_M = \underbrace{(\mathbf{Z}_{M11} - \mathbf{Z}_{M12}(\mathbf{Z} + \mathbf{Z}_{M22})^{-1}\mathbf{Z}_{M21})}_{\mathbf{Z}_T} \mathbf{i}_M, \quad (17)$$

where $\mathbf{Z}_T \in \mathbb{C}^{N \times N}$ is the overall transmit impedance matrix accounting for power matching and mutual coupling. The problem of optimal multiport matching is to find \mathbf{Z}_M so that $\mathbf{Z}_T = Z_s^* \mathbf{I}_N$. In this case, there are no reflection losses and half of the generated power enters the antenna array, i.e., maximum power transfer [27]. This is accomplished for [26]

$$\mathbf{Z}_M = \begin{bmatrix} -j\text{Im}\{Z_s\}\mathbf{I}_N & -j\sqrt{R_s}\text{Re}\{\mathbf{Z}\}^{1/2} \\ -j\sqrt{R_s}\text{Re}\{\mathbf{Z}\}^{1/2} & -j\text{Im}\{\mathbf{Z}\} \end{bmatrix}. \quad (18)$$

Under (18), we have that

$$\mathbf{v}_s = Z_s \mathbf{I}_N \mathbf{i}_M + \mathbf{v}_M = (Z_s \mathbf{I}_N + \mathbf{Z}_T) \mathbf{i}_M = 2R_s \mathbf{i}_M, \quad (19)$$

and the total power generated by the voltage sources is

$$P_{\text{total}} = \frac{1}{2} \text{Re} \{ \mathbf{v}_s^H \mathbf{i}_M \} = R_s \|\mathbf{i}_M\|^2. \quad (20)$$

From (16) and (18), it also holds that

$$\mathbf{i}_M = \mathbf{Z}_{M21}^{-1} (\mathbf{Z} + \mathbf{Z}_{M22}) \mathbf{i} = \frac{j}{\sqrt{R_s}} \text{Re}\{\mathbf{Z}\}^{1/2} \mathbf{i}, \quad (21)$$

and hence $P_{\text{total}} = \mathbf{i}^H \text{Re}\{\mathbf{Z}\} \mathbf{i} = 2P_{\text{in}}$, which confirms the optimality of (18).

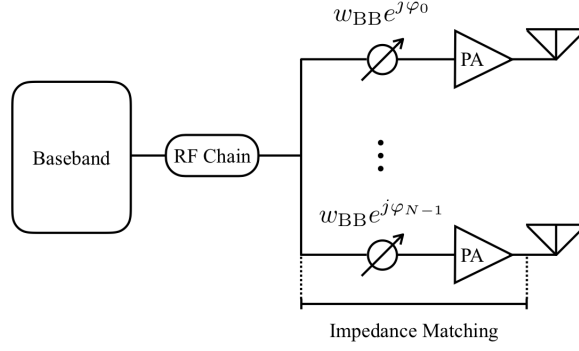


Fig. 3: Illustration of hybrid analog-digital array architecture with a one RF chain.

IV. HARDWARE-EFFICIENT IMPLEMENTATION OF SUPERDIRECTIONAL BEAMSTEERING

In this section, we investigate the problem of generating a superdirective beam with one RF chain and a low-complexity impedance matching network.

A. Problem Statement

From (12), (19), and (21), the vector of voltage sources maximizing the array gain is given by

$$\begin{aligned} \mathbf{v}_s^* &= 2R_s \mathbf{i}_M^* = j2\sqrt{R_s} \text{Re}\{\mathbf{Z}\}^{1/2} \mathbf{i}^* \\ &= j2\sqrt{\frac{2R_s P_t}{\mathbf{a}^H(\theta) \text{Re}\{\mathbf{Z}\}^{-1} \mathbf{a}(\theta)}} \text{Re}\{\mathbf{Z}\}^{-1/2} \mathbf{a}(\theta). \end{aligned} \quad (22)$$

In most massive MIMO studies, a signal processing-based approach is usually followed wherein beamforming is described by a $N \times 1$ complex vector \mathbf{w} . Following the approach in [28], the optimal vector \mathbf{w} is calculated from the physical source voltages through the relationship

$$\mathbf{w} = -\frac{1}{j2\sqrt{R_s}} (\mathbf{v}_s^*)^* = \sqrt{\frac{2P_t}{\mathbf{a}^H(\theta) \text{Re}\{\mathbf{Z}\}^{-1} \mathbf{a}(\theta)}} \text{Re}\{\mathbf{Z}\}^{-1/2} \mathbf{a}^*(\theta). \quad (23)$$

We next consider a hybrid analog-digital array architecture with one RF chain and N analog phase shifters, as shown in Fig. 3. In this case, $\mathbf{w} = w_{\text{BB}} [e^{j\varphi_0}, \dots, e^{j\varphi_{N-1}}]^T$, where w_{BB} denotes the complex amplitude of baseband processing whilst $\{\varphi_n\}_{n=0}^{N-1}$ are the variable phases. Consequently, beamsteering requires voltage sources $\{v_{s,n}\}_{n=0}^{N-1}$ of the same magnitude. From (22), it is easy to verify that \mathbf{v}_s^* has entries of different magnitudes, and hence cannot be realized by a single RF chain. In summary, superdirective ULAs require amplitude control at each antenna, which can be provided by a fully digital array or an active phased array with digitally controlled amplitude attenuators. However, those architectures substantially increase hardware complexity and power consumption. Similarly, multiport matching requires interconnections and

circuit components between all the $2N$ ports [29]. Thus, it is prohibitively complex for a large number N of antennas [30].

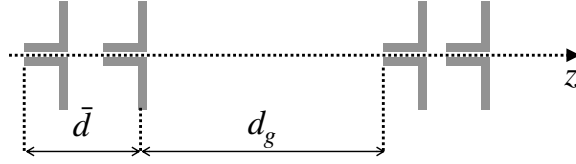


Fig. 4: Example of a NULA with $N_g = 2$ and $\bar{N} = 2$.

B. Proposed Solution

1) *Nonuniform Linear Array*: The BS array is divided into N_g groups of \bar{N} antennas each, i.e., $N = N_g \bar{N}$. Let d_g and \bar{d} denote the inter-group and inter-element spacings, respectively, as shown in Fig. 4. The distance of the \bar{n} th element in the n_g th subarray from the origin of the coordinate system is given by $(\bar{n}\bar{d} + n_g(d_g + (\bar{N} - 1)\bar{d})) \cos \theta$, where $\bar{n} = 0, \dots, \bar{N} - 1$ and $n_g = 0, \dots, N_g - 1$. Thus, the array response vector $\mathbf{a}(\theta)$ can be recast as

$$\begin{aligned} \mathbf{a}(\theta) &= \left[\mathbf{a}_0(\theta), \mathbf{a}_0(\theta) e^{-j\kappa((d_g + (\bar{N} - 1)\bar{d}) \cos \theta)}, \dots, \right. \\ &\quad \left. \mathbf{a}_0(\theta) e^{-j\kappa(N_g - 1)(d_g + (\bar{N} - 1)\bar{d}) \cos \theta} \right]^T \\ &= \mathbf{a}_g(\theta) \otimes \mathbf{a}_0(\theta), \end{aligned} \quad (24)$$

where $\mathbf{a}_0(\theta) \triangleq [1, \dots, e^{-j\kappa(\bar{N} - 1)\bar{d} \cos \theta}]^T \in \mathbb{C}^{\bar{N} \times 1}$ is the response vector of the 0th antenna group, and $\mathbf{a}_g(\theta) \triangleq [1, \dots, e^{-j\kappa(N_g - 1)(d_g + (\bar{N} - 1)\bar{d}) \cos \theta}]^T \in \mathbb{C}^{N_g \times 1}$ is the response vector between groups. Similarly, the input impedance matrix is partitioned as

$$\mathbf{Z} = \begin{bmatrix} \mathbf{Z}_0 & \mathbf{Z}_{0,1} & \cdots & \mathbf{Z}_{0,N_g-1} \\ \mathbf{Z}_{1,0} & \mathbf{Z}_0 & \cdots & \mathbf{Z}_{1,N_g-1} \\ \vdots & \vdots & \ddots & \vdots \\ \mathbf{Z}_{N_g-1,0} & \mathbf{Z}_{N_g-1,1} & \cdots & \mathbf{Z}_0 \end{bmatrix}, \quad (25)$$

where $\text{Re}\{\mathbf{Z}_{n_{g1}, n_{g2}}\} \in \mathbb{R}^{\bar{N} \times \bar{N}}$ is defined as

$$\text{Re}\{\mathbf{Z}_{n_{g1}, n_{g2}}\} \triangleq \frac{\eta}{4\pi^2} \int_0^\pi \int_0^{2\pi} \mathbf{a}_0(\theta) \mathbf{a}_0^H(\theta) e^{-j\kappa(n_{g1} - n_{g2})(d_g + (\bar{N} - 1)\bar{d}) \cos \theta} \|\mathbf{F}(\theta)\|^2 \sin \theta d\theta d\phi, \quad \text{for } n_{g1} \neq n_{g2}, \quad (26)$$

and

$$\text{Re}\{\mathbf{Z}_0\} = \frac{\eta}{4\pi^2} \int_0^\pi \int_0^{2\pi} \mathbf{a}_0(\theta) \mathbf{a}_0^H(\theta) \|\mathbf{F}(\theta)\|^2 \sin\theta d\theta d\phi + R_{\text{loss}} \mathbf{I}_{\bar{N}}, \quad \text{for } n_{g1} = n_{g2}. \quad (27)$$

In fact, \mathbf{Z}_0 corresponds to the input impedance matrix of each \bar{N} -element group. For $\bar{N} = 2$, we have that

$$\text{Re}\{\mathbf{Z}_0\} \triangleq \begin{bmatrix} R_{\text{self}} & R_m \\ R_m & R_{\text{self}} \end{bmatrix}, \quad (28)$$

where $R_{\text{self}} = R_{\text{loss}} + R_i$ denotes the self impedance for notational convenience, and R_m is the real part of the mutual impedance between two adjacent dipoles.

When the inter-group spacing is sufficiently large, the coupling between groups can be neglected. Thus, $\text{Re}\{\mathbf{Z}_{n_{g1}, n_{g2}}\} \approx \mathbf{0}_{\bar{N} \times \bar{N}}$ for $n_{g1} \neq n_{g2}$, which makes \mathbf{Z} approximately a block diagonal matrix, namely $\text{Re}\{\mathbf{Z}\} \approx \mathbf{I}_{N_g} \otimes \text{Re}\{\mathbf{Z}_0\} = \text{Re}\{\mathbf{Z}_{\text{approx}}\}$. We finally stress that in addition to a large d_g , the mutual coupling between antenna groups can be further reduced through a decoupling technique, such as electromagnetic bandgap structures placed between them [31].

2) *Coupled Antenna Pairs* : A major drawback of beamsteering under mutual coupling is the requirement of amplitude control at each voltage source. However, in a NULA, all antenna groups share the same voltage amplitudes. This is because from (22)

$$\begin{aligned} \mathbf{v}_s^* &= \bar{v} \text{Re}\{\mathbf{Z}\}^{-1/2} \mathbf{a}(\theta) \approx \bar{v} \text{Re}\{\mathbf{Z}_{\text{approx}}\}^{-1/2} \mathbf{a}(\theta) \\ &= \bar{v} (\mathbf{I}_{N_g} \otimes \text{Re}\{\mathbf{Z}_0\}^{-1/2}) (\mathbf{a}_g(\theta) \otimes \mathbf{a}_0(\theta)) \\ &= \bar{v} \mathbf{a}_g(\theta) \otimes (\text{Re}\{\mathbf{Z}_0\}^{-1/2} \mathbf{a}_0(\theta)), \end{aligned} \quad (29)$$

where $\bar{v} = j2\sqrt{2R_s P_t / \mathbf{a}^H(\theta_k) \text{Re}\{\mathbf{Z}\}^{-1} \mathbf{a}(\theta_k)}$, which gives

$$\text{mag}(\mathbf{v}_s^*) = \bar{v} \begin{bmatrix} \text{mag}(\text{Re}\{\mathbf{Z}_0\}^{-1/2} \mathbf{a}_0(\theta)) \\ \vdots \\ \text{mag}(\text{Re}\{\mathbf{Z}_0\}^{-1/2} \mathbf{a}_0(\theta)) \end{bmatrix}. \quad (30)$$

By exploiting that property of NULAs, we further propose two-element groups. The following proposition justifies the choice of $\bar{N} = 2$.

Proposition 1. For $\bar{N} = 2$, it holds that

$$\begin{aligned} & \text{mag}(\text{Re}\{\mathbf{Z}_0\}^{-1/2}\mathbf{a}_0(\theta)) = \\ & = \mathbf{1}_{2 \times 1} \frac{1}{\sqrt{2R_{\text{self}} + 2\sqrt{R_{\text{self}}^2 - R_m^2}}} \\ & \times \sqrt{\left(\frac{R_{\text{self}}}{\sqrt{R_{\text{self}}^2 - R_m^2}} + 1\right)^2 + \frac{R_m^2}{R_{\text{self}}^2 - R_m^2} - 2\left(\frac{R_{\text{self}}}{\sqrt{R_{\text{self}}^2 - R_m^2}} + 1\right)\frac{R_m}{\sqrt{R_{\text{self}}^2 - R_m^2}}\cos(\kappa\bar{d}\cos\theta)}. \end{aligned} \quad (31)$$

Proof. See Appendix B. □

According to Proposition 1, antenna pairs result in *uniform* amplitudes $\{|v_{s,n}|\}_{n=0}^{N-1}$, thereby enabling the realization of superdirective beamsteering with a single RF chain and N analog phase shifters. Additionally, each antenna pair is separately matched using the four-port network (see Appendix C)

$$\mathbf{Z}_{M,0} = \begin{bmatrix} -j\text{Im}\{Z_s\}\mathbf{I}_2 & -j\sqrt{R_s}\text{Re}\{\mathbf{Z}_0\}^{1/2} \\ -j\sqrt{R_s}\text{Re}\{\mathbf{Z}_0\}^{1/2} & -j\text{Im}\{\mathbf{Z}_0\} \end{bmatrix}. \quad (32)$$

Therefore, the proposed solution also facilitates the implementation of optimal multiport matching, which would not be possible in a coupled ULA with a large number of elements.

V. THZ MASSIVE MIMO MODEL

In this section, we introduce the high-level system model used to evaluate the performance of the proposed NULA in terms of achievable rate and EE.

A. Signal Model

Consider a THz massive MIMO system, where the BS serves $K \ll N$ single-antenna users. Let $\mathbf{h}_k \in \mathbb{C}^{N \times 1}$ and β_k denote the small-scale fading channel and path loss of user k , respectively. The downlink channel of user k is then specified as $\sqrt{\beta_k}\mathbf{h}_k^T$. To facilitate hardware implementation, a fully connected analog-digital array with N_{RF} RF chains is considered at the BS [32]. Thus, the precoder is decomposed as $\mathbf{W} = \mathbf{W}_{\text{RF}}\mathbf{W}_{\text{BB}} = [\mathbf{w}_1, \dots, \mathbf{w}_{N_{\text{RF}}}] \in \mathbb{C}^{N \times N_{\text{RF}}}$, where $\mathbf{W}_{\text{RF}} \in \mathbb{C}^{N \times N_{\text{RF}}}$ is the RF beamformer realized by analog phase shifters, whereas $\mathbf{W}_{\text{BB}} \in \mathbb{C}^{N_{\text{RF}} \times N_{\text{RF}}}$ is the baseband precoder. Without loss of generality, we assume $N_{\text{RF}} = K$ hereafter. Let $\mathbf{x} = [x_1, \dots, x_K]^T \sim \mathcal{CN}(\mathbf{0}_{K \times 1}, \mathbf{I}_K)$ be the vector

of users' data symbols. The transmitted signal is then given by $\mathbf{W}\mathbf{x} \in \mathbb{C}^{N \times 1}$, and should satisfy the power constraint

$$\mathbb{E} \{ \|\mathbf{W}\mathbf{x}\|^2 \} = \sum_{k=1}^K \|\mathbf{w}_k\|^2 \leq 2P_t, \quad (33)$$

where $2P_t$ is the *total power* under perfect impedance matching. Given the above, the received baseband signal at the k th user is written as

$$y_k = \sqrt{\beta_k} \mathbf{h}_k^T \mathbf{w}_k x_k + \sqrt{\beta_k} \sum_{i=1, i \neq k}^K \mathbf{h}_k^T \mathbf{w}_i x_i + n_k, \quad (34)$$

where $n_k \sim \mathcal{CN}(0, \sigma^2)$ is the additive noise. Finally, the signal-to-interference-plus-noise ratio (SINR) of user k is

$$\text{SINR}_k = \frac{\beta_k |\mathbf{h}_k^T \mathbf{w}_k|^2}{\beta_k \sum_{i=1, i \neq k}^K |\mathbf{h}_k^T \mathbf{w}_i|^2 + B\sigma^2}, \quad (35)$$

where $B\sigma^2$ is the noise power over the transmit bandwidth B .

B. Channel Model

Because of the severe path attenuation in the THz band, multi-path scattering is very limited. We therefore assume line-of-sight (LoS) links between the BS and users, akin to [33]. In the presence of mutual coupling at the BS array, the channel vector of user k is expressed as [26, Eq. (105)]

$$\mathbf{h}_k \triangleq \text{Re} \{ \bar{\mathbf{Z}} \}^{-1/2} \mathbf{a}(\theta_k), \quad (36)$$

where $\bar{\mathbf{Z}} \triangleq \frac{1}{R_{\text{loss}} + R_i} \mathbf{Z}$ is the *normalized* input impedance matrix of the BS array.² Finally, because the molecular absorption losses are no longer negligible at THz frequencies, the path loss coefficient is calculated as [34]

$$\beta_k = G_e(\theta_k, \phi_k) \left(\frac{\lambda}{4\pi r_k} \right)^2 e^{-\kappa_{\text{abs}} r_k}, \quad (37)$$

where $G_e(\theta_k, \phi_k)$ is the gain of each BS antenna, λ is the carrier wavelength, r_k is the distance from the BS to user k , and κ_{abs} is the molecular absorption coefficient determined by the composition of the propagation medium [35].

²The normalized input impedance matrix is used for notational convenience. In this way, the array gain is recast as $G(\theta, \phi) = G_e(\theta, \phi) \frac{|\mathbf{a}^H(\theta)|^2}{i^H \text{Re} \{ \bar{\mathbf{Z}} \} \mathbf{1}}$, and the path loss coefficient or channel vector will not include the term $R_{\text{loss}} + R_i$. For example, $\text{Re} \{ \bar{\mathbf{Z}} \} = \mathbf{I}_N$ and $\mathbf{h}_k = \mathbf{a}(\theta_k)$ in the absence of coupling.

C. Power Consumption Model

For a fully-connected array structure, the overall power consumption is given by [36]

$$P_c = P_{\text{BB}} + KP_{\text{RF}} + KN P_{\text{PS}} + NP_{\text{PA}} + P_t + P_{\text{CE}}, \quad (38)$$

where P_{BB} , P_{RF} , P_{PS} , P_{PA} , and P_{CE} denote the powers consumed by a baseband unit, an RF chain, a phase shifter, a power amplifier, and the channel estimation process, respectively. Moreover, each RF chain comprises a digital-to-analog converter (DAC), a local oscillator, and a mixer, and hence $P_{\text{RF}} = P_{\text{DAC}} + P_{\text{LO}} + P_{\text{M}}$. We finally stress that the power consumption of splitters and combiners is negligible, and hence is ignored [36].

VI. SIGNAL AND INTERFERENCE POWERS

A. Proposed NULA

We consider MRT at the BS. Under equal power allocation, we have that

$$\mathbf{w}_k = \sqrt{\frac{2P_t}{K}} \frac{\mathbf{h}_k^*}{\|\mathbf{h}_k\|} = \sqrt{\frac{2P_t}{K \mathbf{a}^H(\theta_k) \text{Re}\{\bar{\mathbf{Z}}\}^{-1} \mathbf{a}(\theta_k)}} \text{Re}\{\bar{\mathbf{Z}}\}^{-\frac{1}{2}} \mathbf{a}^*(\theta_k), \quad (39)$$

and the power of the desired signal, normalized by $K/(2P_t)$, is

$$\frac{K}{2P_t} |\mathbf{h}_k^T \mathbf{w}_k|^2 = \mathbf{a}^H(\theta_k) \text{Re}\{\bar{\mathbf{Z}}\}^{-1} \mathbf{a}(\theta_k). \quad (40)$$

Due to the block-diagonal structure of $\bar{\mathbf{Z}}$, (40) simplifies to

$$\begin{aligned} \frac{K}{2P_t} |\mathbf{h}_k^T \mathbf{w}_k|^2 &\approx \mathbf{a}^H(\theta_k) \text{Re}\{\bar{\mathbf{Z}}_{\text{approx}}\}^{-1} \mathbf{a}(\theta_k) \\ &= (\mathbf{a}_g^H(\theta_k) \otimes \mathbf{a}_0^H(\theta_k)) (\mathbf{I}_{N_g} \otimes \text{Re}\{\bar{\mathbf{Z}}_0\}^{-1}) (\mathbf{a}_g(\theta_k) \otimes \mathbf{a}_0(\theta_k)) \\ &= N_g \mathbf{a}_0^H(\theta_k) \text{Re}\{\bar{\mathbf{Z}}_0\}^{-1} \mathbf{a}_0(\theta_k), \end{aligned} \quad (41)$$

where $\bar{\mathbf{Z}}_{\text{approx}} = \frac{1}{R_{\text{loss}} + R_i} \mathbf{Z}_{\text{approx}}$ and $\bar{\mathbf{Z}}_0 = \frac{1}{R_{\text{loss}} + R_i} \mathbf{Z}_0$. As seen from (41), the power gain of the NULA is N_g times the gain of a superdirective antenna group. In the sequel, we determine $\mathbf{a}_0^H(\theta_k) \text{Re}\{\bar{\mathbf{Z}}_0\}^{-1} \mathbf{a}_0(\theta_k)$ in closed-form for $\bar{N} = 2$. We first have that

$$\text{Re}\{\bar{\mathbf{Z}}_0\} = \begin{bmatrix} 1 & \bar{R}_m \\ \bar{R}_m & 1 \end{bmatrix}, \quad (42)$$

where $\bar{R}_m = \frac{1}{R_{\text{loss}} + R_i} R_m$. Then, the inverse matrix is determined as

$$\text{Re} \{ \bar{\mathbf{Z}}_0 \}^{-1} = \frac{1}{1 - \bar{R}_m^2} \begin{bmatrix} 1 & -\bar{R}_m \\ -\bar{R}_m & 1 \end{bmatrix}, \quad (43)$$

and

$$\text{Re} \{ \bar{\mathbf{Z}}_0 \}^{-1} \mathbf{a}_0(\theta_k) = \frac{1}{1 - \bar{R}_m^2} \begin{bmatrix} 1 & -\bar{R}_m \\ -\bar{R}_m & 1 \end{bmatrix} \begin{bmatrix} 1 \\ e^{-j\kappa\bar{d}\cos\theta_k} \end{bmatrix} = \frac{1}{1 - \bar{R}_m^2} \begin{bmatrix} 1 - \bar{R}_m e^{-j\kappa\bar{d}\cos\theta_k} \\ -\bar{R}_m + e^{-j\kappa\bar{d}\cos\theta_k} \end{bmatrix}, \quad (44)$$

which gives

$$\begin{aligned} \mathbf{a}_0^H(\theta_k) \text{Re} \{ \bar{\mathbf{Z}}_0 \}^{-1} \mathbf{a}_0(\theta_k) &= \frac{1}{1 - \bar{R}_m^2} \left(1 - \bar{R}_m e^{-j\kappa\bar{d}\cos\theta_k} - \bar{R}_m e^{j\kappa\bar{d}\cos\theta_k} + 1 \right) \\ &= \frac{2}{1 - \bar{R}_m^2} \left(1 - \bar{R}_m \cos(\kappa\bar{d}\cos\theta_k) \right). \end{aligned} \quad (45)$$

According to (45), $\mathbf{a}_0^H(\theta_k) \text{Re} \{ \bar{\mathbf{Z}}_0 \}^{-1} \mathbf{a}_0(\theta_k) \approx 2$ for large \bar{d} , i.e., $\bar{R}_m \approx 0$, which corresponds to the conventional power gain of a two-element array.

Similarly, the interference power at user k from the beam toward user $i \neq k$, normalized by $K/(2P_t)$, is given by

$$\begin{aligned} \frac{K}{2P_t} |\mathbf{h}_k^T \mathbf{w}_i|^2 &= \frac{|\mathbf{a}_0^H(\theta_k) \text{Re} \{ \bar{\mathbf{Z}} \}^{-1} \mathbf{a}(\theta_i)|^2}{\mathbf{a}_0^H(\theta_i) \text{Re} \{ \bar{\mathbf{Z}} \}^{-1} \mathbf{a}(\theta_i)} \approx \frac{|\mathbf{a}_0^H(\theta_k) \text{Re} \{ \bar{\mathbf{Z}}_{\text{approx}} \}^{-1} \mathbf{a}(\theta_i)|^2}{\mathbf{a}_0^H(\theta_i) \text{Re} \{ \bar{\mathbf{Z}}_{\text{approx}} \}^{-1} \mathbf{a}(\theta_i)} \\ &\stackrel{(a)}{=} N_g |D_{N_g}(\kappa(d_g + (\bar{N} - 1)\bar{d})(\cos\theta_k - \cos\theta_i))|^2 \\ &\quad \times \frac{|\mathbf{a}_0^H(\theta_k) \text{Re} \{ \bar{\mathbf{Z}}_0 \}^{-1} \mathbf{a}_0(\theta_i)|^2}{\mathbf{a}_0^H(\theta_i) \text{Re} \{ \bar{\mathbf{Z}}_0 \}^{-1} \mathbf{a}_0(\theta_i)}, \end{aligned} \quad (46)$$

where (a) is proven in Appendix D. From (44) and (45), we finally have that

$$\frac{|\mathbf{a}_0^H(\theta_k) \text{Re} \{ \bar{\mathbf{Z}}_0 \}^{-1} \mathbf{a}_0(\theta_i)|^2}{\mathbf{a}_0^H(\theta_i) \text{Re} \{ \bar{\mathbf{Z}}_0 \}^{-1} \mathbf{a}_0(\theta_i)} = \frac{|1 + e^{j\kappa\bar{d}(\cos\theta_k - \cos\theta_i)} - \bar{R}_m (e^{j\kappa\bar{d}\cos\theta_k} + e^{-j\kappa\bar{d}\cos\theta_i})|^2}{2(1 - \bar{R}_m^2) (1 - \bar{R}_m \cos(\kappa\bar{d}\cos\theta_i))}. \quad (47)$$

B. Comparison With Uncoupled ULA

In the massive MIMO literature, it is customary to consider a uniform inter-element spacing [37]. Furthermore, mutual coupling is avoided by employing a sufficiently large d so that $\text{Re} \{ \bar{\mathbf{Z}} \} \approx \mathbf{I}_N$. In this

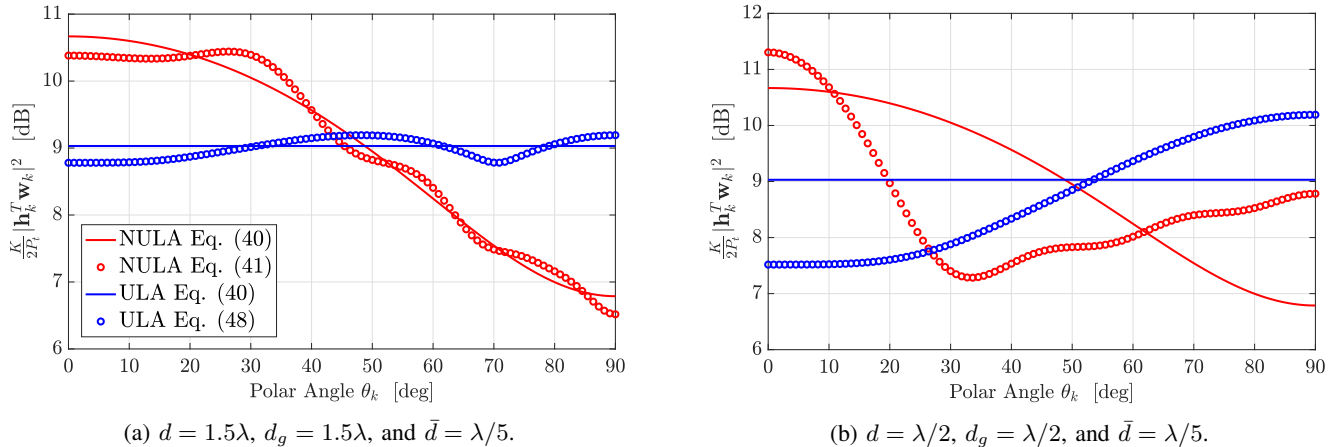


Fig. 5: Normalized signal power versus polar angle for $N = 8$ dipoles of $\ell = \lambda/2$, $\rho = \lambda/500$, and $\sigma_c = 5.7 \times 10^7$ S/m. In NULA, $\bar{N} = 2$ and $N_g = 4$. The carrier frequency is set to $f = 300$ GHz.

case, the normalized power of the desired signal becomes

$$\frac{K}{2P_t} |\mathbf{h}_k^T \mathbf{w}_k|^2 \approx N, \quad (48)$$

whereas the normalized interference is

$$\frac{K}{2P_t} |\mathbf{h}_k^T \mathbf{w}_i|^2 \approx N |D_N(\kappa d(\cos \theta_k - \cos \theta_i))|^2. \quad (49)$$

From (48), it is evident that the power gain is independent of the steering direction θ_k in an uncoupled ULA. This assumption is safely made for a large antenna separation, as showcased in Fig. 5. Specifically, half-wavelength spacing does create coupling between directional antennas, and hence the input impedance matrix cannot be ignored.³ Lastly, according to the approximate expressions, the proposed NULA with $\bar{N} = 2$ yields a *relative* power gain equal to

$$N_g \mathbf{a}_0^H(\theta_k) \text{Re} \{ \bar{\mathbf{Z}}_0 \}^{-1} \mathbf{a}_0(\theta_k) - N = N_g \left[\mathbf{a}_0^H(\theta_k) \text{Re} \{ \bar{\mathbf{Z}}_0 \}^{-1} \mathbf{a}_0(\theta_k) - 2 \right] = O(N_g), \quad (50)$$

which scales linearly with N_g for some $\theta_k \in [0, \theta_{\max}]$; for example, $\theta_{\max} \approx 50^\circ$ in Fig. 5(a). This trade off between directivity and angular coverage is fundamental [39]. Thus, increasing the former inevitably decreases the latter, and vice versa. Whether it is beneficial to have a highly directive array depends on the propagation environment and deployment scenario [39], [40].

³The assumption of uncoupled elements under half-wavelength spacing holds only for isotropic radiators [38].

VII. CHANNEL ESTIMATION

So far, we have assumed perfect channel knowledge at the BS and analyzed the performance of MRT in the presence of mutual coupling. In this section, we focus on the channel estimation problem, which is crucial to beamforming.

A. Channel Reciprocity

In massive MIMO, it is typical to invoke channel reciprocity for time-division duplex (TDD) operation [41]. This enables the BS to estimate the downlink channel through uplink pilots sent by users. Let $\mathbf{h}_{k,\text{DL}} = \mathbf{h}_k^T \in \mathbb{C}^{1 \times N}$ denote the downlink channel, where \mathbf{h}_k is given by (36). The TDD assumption is then that $\mathbf{h}_{k,\text{UL}} = \mathbf{h}_{k,\text{DL}}^T$. Although the physical channels (i.e., those defined by electromagnetic theory) are reciprocal, this does not generally hold for their information-theoretic counterparts in the presence of antenna mutual coupling [42]. In particular, the BS needs to employ a linear transformation to compute $\mathbf{h}_{k,\text{DL}}^T$ from the estimated $\mathbf{h}_{k,\text{UL}}$. Nevertheless, the transmit and receive array gains coincide with each other under isotropic background noise and noise matching at the receiver [26, Eq. (97)]. Thus, we can assume that $\mathbf{h}_{k,\text{UL}} = \mathbf{h}_{k,\text{DL}}^T$, and that the reception strategy maximizing the signal-to-noise ratio (SNR) of each user k is the maximum ratio combiner $\mathbf{v}_k = \mathbf{h}_k^H / \|\mathbf{h}_k\|$.

B. Problem Formulation

We assume a block-fading model, where the channel coherence time is much larger than the training period. The BS estimates the uplink channel \mathbf{h}_k of each user k in rounds. Subsequently, we focus on an arbitrary user and omit the subscript “ k ”. Specifically, the training period for each user consists of N_{slot} time slots. At each time slot $t = 1, \dots, N_{\text{slot}}$, the user transmits the pilot signal $x_t = \sqrt{P_p}$, where P_p is the power per pilot signal. In turn, the BS combines the received pilot signal using a training hybrid combiner $\mathbf{V}_t = \mathbf{V}_{\text{RF},t} \mathbf{V}_{\text{BB},t} \in \mathbb{C}^{N \times N_{\text{RF}}}$. Therefore, the post-processed signal at slot t , $\mathbf{y}_t \in \mathbb{C}^{K \times 1}$, is written as

$$\mathbf{y}_t = \sqrt{\beta P_p} \mathbf{V}_t^H \mathbf{h} + \mathbf{V}_t^H \mathbf{n}_t, \quad (51)$$

where $\mathbf{n}_t \sim \mathcal{CN}(\mathbf{0}_{N \times 1}, \sigma^2 \mathbf{I}_N)$ is the additive noise vector. Let $N_{\text{beam}} = N_{\text{slot}} N_{\text{RF}}$ denote the total number of pilot beams. After N_{slot} training slots, the BS acquires the measurement vector $\bar{\mathbf{y}} \triangleq [\mathbf{y}_1^T, \dots, \mathbf{y}_{N_{\text{slot}}}^T]^T \in$

$\mathbb{C}^{N_{\text{beam}} \times 1}$ for \mathbf{h} as

$$\bar{\mathbf{y}} = \sqrt{\beta P_p} \begin{bmatrix} \mathbf{V}_1^H \\ \vdots \\ \mathbf{V}_{N_{\text{slot}}}^H \end{bmatrix} \mathbf{h} + \begin{bmatrix} \mathbf{V}_1^H \mathbf{n}_1 \\ \vdots \\ \mathbf{V}_{N_{\text{slot}}}^H \mathbf{n}_{N_{\text{slot}}} \end{bmatrix} = \sqrt{\beta P_p} \bar{\mathbf{V}}^H \mathbf{h} + \bar{\mathbf{n}}, \quad (52)$$

where $\bar{\mathbf{V}} \triangleq [\mathbf{V}_1, \dots, \mathbf{V}_{N_{\text{slot}}}] \in \mathbb{C}^{N \times N_{\text{beam}}}$, whereas $\bar{\mathbf{n}} \in \mathbb{C}^{N_{\text{beam}} \times 1}$ is the effective noise. More particularly, $\mathbf{R}_{\bar{\mathbf{n}}[s]} \triangleq \sigma^2 \text{blkdiag}(\mathbf{V}_1^H \mathbf{V}_1, \dots, \mathbf{V}_{N_{\text{slot}}}^H \mathbf{V}_{N_{\text{slot}}})$ is the covariance matrix of the effective noise, which is colored in general.⁴ Regarding the pilot combiners, due to the hybrid array architecture, $\bar{\mathbf{V}} = \bar{\mathbf{V}}_{\text{RF}} \bar{\mathbf{V}}_{\text{BB}}$, with $\bar{\mathbf{V}}_{\text{RF}} = [\mathbf{V}_{\text{RF},1}, \dots, \mathbf{V}_{\text{RF},N_{\text{slot}}}] \in \mathbb{C}^{N \times N_{\text{beam}}}$ and $\bar{\mathbf{V}}_{\text{BB}} = \text{blkdiag}(\mathbf{V}_{\text{BB},1}, \dots, \mathbf{V}_{\text{BB},N_{\text{slot}}}) \in \mathbb{C}^{N_{\text{beam}} \times N_{\text{beam}}}$ comprising the pilot RF beams and baseband combiners of the N_{slot} time slots, respectively.

C. Orthogonal Matching Pursuit

1) *Sparse Formulation*: We next consider a dictionary $\bar{\mathbf{H}} \in \mathbb{C}^{N \times G}$ whose G columns are the channel vectors associated with a predefined set of angles-of-arrival (AoA). Then, the uplink channel can be approximated as

$$\mathbf{h} \approx \bar{\mathbf{H}} \boldsymbol{\beta}, \quad (53)$$

where $\boldsymbol{\beta}$ is a $G \times 1$ vector with a single nonzero entry corresponding to the LoS path. Therefore, (52) is recast as $\bar{\mathbf{y}} \approx \Phi \boldsymbol{\beta} + \bar{\mathbf{n}}$, where $\Phi \triangleq \sqrt{P_p} \bar{\mathbf{V}}^H \bar{\mathbf{H}} \in \mathbb{C}^{N_{\text{beam}} \times G}$ is the *equivalent* sensing matrix. Since $G \gg 1$, the vector $\bar{\boldsymbol{\beta}}$ is 1-sparse, and thus the channel estimation problem can be formulated as the sparse recovery problem [43]

$$\hat{\boldsymbol{\beta}} = \arg \min_{\boldsymbol{\beta}} \|\boldsymbol{\beta}\|_1 \quad \text{subject to} \quad \|\bar{\mathbf{y}} - \Phi \boldsymbol{\beta}\| \leq \epsilon, \quad (54)$$

where $\epsilon \leq \mathbb{E}\{\|\bar{\mathbf{n}}\|\}$ is an appropriately chosen bound on the mean magnitude of the effective noise. The l_1 -norm optimization problem in (54) can be readily solved by the popular OMP algorithm, which takes the following form for single-path channels

$$g^* = \arg \max_{g \in \mathcal{G}} |\Phi^H(g) \bar{\mathbf{y}}|, \quad (55)$$

where \mathcal{G} denotes the set of predefined AoA. Finally, the estimate of \mathbf{h} is obtained as $\hat{\mathbf{h}} = \bar{\mathbf{H}}(g^*)$. It is worth stressing that the actual AoA might differ from the one defined by the dictionary. Nonetheless, this

⁴We have assumed the same noise variance, σ^2 , as in the user side.

mismatch error can become negligible by adopting a high-resolution dictionary, as demonstrated in [43].

2) *Dictionary for NULAs and Pilot Beams*: In the spirit of [44], [45], we discretize the polar angle $\theta \in [0, \theta_{\max}]$ as

$$\bar{\theta}_g = \frac{\theta_{\max}}{G}g, \quad g = 0, \dots, G-1, \quad (56)$$

which results in the coupling-aware dictionary

$$\bar{\mathbf{H}} = \left[\text{Re}\{\mathbf{Z}\}^{-\frac{1}{2}} \mathbf{a}(\bar{\theta}_0), \dots, \text{Re}\{\mathbf{Z}\}^{-\frac{1}{2}} \mathbf{a}(\bar{\theta}_{G-1}) \right]. \quad (57)$$

The elements of the RF combiner $\bar{\mathbf{V}}_{\text{RF}}$ are selected from the set $\{-1/\sqrt{N}, 1/\sqrt{N}\}$ with equal probability. The reason we adopt a randomly formed RF combiner is that it will exhibit low mutual-column coherence, and therefore is expected to attain a high recovery probability according to the compressed sensing (CS) theory [46]. The columns of $\bar{\mathbf{V}}_{\text{RF}}$ have been normalized so that the total power consumed during the channel estimation stage is

$$P_{\text{CE}} = KN_{\text{beam}}P_p, \quad (58)$$

as KN_{beam} pilot beams are used for the K users.

The specific RF pilot design results in a colored effective noise. For this reason, we design the baseband combiner such that the effective noise remains white. Let $\mathbf{D}_t^H \mathbf{D}_t$ be the Cholesky decomposition of $\mathbf{V}_{\text{RF},t}^H \mathbf{V}_{\text{RF},t}$, where $\mathbf{D} \in \mathbb{C}^{N_{\text{RF}} \times N_{\text{RF}}}$ is an upper triangular matrix. Then, the baseband combiner of the t th slot is set to $\mathbf{V}_{\text{BB},t} = \mathbf{D}_t^{-1}$, and hence $\bar{\mathbf{V}} = \bar{\mathbf{V}}_{\text{RF}} \text{blkdiag}(\mathbf{D}_1^{-1}, \dots, \mathbf{D}_{N_{\text{slot}}}^{-1})$. Under this pilot beam design, the covariance matrix of the effective noise becomes $\mathbf{R}_{\bar{\mathbf{n}}} = \sigma^2 \mathbf{I}_{N_{\text{beam}}}$.

VIII. REDUCING THE NUMBER OF BS ANTENNAS

A. Power Gain Versus Spatial Resolution

As demonstrated in Section VI-B, the proposed NULA achieves larger gain than ULA thanks to the superdirective pairs. This excessive power gain can improve EE, as the number of antennas is kept fixed in both array designs. A more radical approach is to employ a NULA with a smaller number of elements than ULA to substantially reduce the power consumption. To see this, consider the overall signal and interference powers

$$\beta_k |\mathbf{h}_k^T \mathbf{w}_k|^2 \propto G(\theta_k, \phi_k) |\mathbf{h}_k^T \mathbf{w}_k|^2, \quad (59)$$

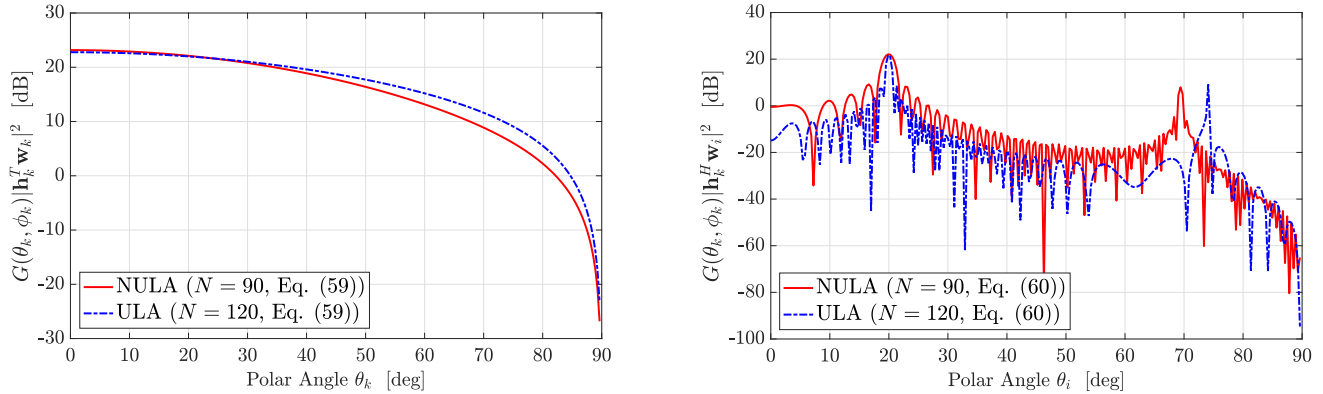


Fig. 6: Signal and interference powers. In NULA, $\bar{N} = 2$, $N_g = 45$, $\bar{d} = \lambda/5$, and $d_g = 1.5\lambda$. In ULA, $N = 120$ and $d = 1.5\lambda$. The interference power is computed for $(\theta_k, \phi_k) = (20^\circ, 0^\circ)$. The other parameters are $P_t = 1/2$, $K = 1$, and $f = 300$ GHz.

and

$$\beta_k |\mathbf{h}_k^T \mathbf{w}_i|^2 \propto G(\theta_k, \phi_k) |\mathbf{h}_k^T \mathbf{w}_i|^2. \quad (60)$$

We now compare an 120-element ULA with an 90-element NULA. In Fig. 6, we confirm that both arrays offer a similar signal power. More importantly, this is accomplished with 30 elements less, which corresponds to a 25% saving in RF hardware. On the other hand, the interference power hinges on d_g , i.e., see (46), which determines the spatial resolution of the array. In the NULA, the spacing d_g is equal to the inter-element spacing of ULA. Specifically, it is set to $d_g = d = 1.5\lambda$ so that strong sidelobes are avoided.⁵ Given that, the NULA with reduced number of elements is shorter and has coarser spatial resolution than the ULA, as showcased in Fig. 6.⁶ The impact of reducing the number of BS antennas on the performance of multiuser transmissions is hard to analytically study, either assuming perfect or imperfect CSI at the BS. For this reason, we resort to numerical simulations in Section IX. Note, though, that the wider beamwidth of NULA favors single-user transmissions under beam alignment errors. Regarding the array dimensions, the lengths of ULA and NULA are given, respectively, by

$$L_{\text{ULA}} = (N - 1)d, \quad (61)$$

$$L_{\text{NULA}} = N_g(\bar{N} - 1)\bar{d} + (N_g - 1)d_g. \quad (62)$$

In the numerical example of Fig. 6, $L_{\text{ULA}} = 17.85$ cm and $L_{\text{NULA}} = 7.5$ cm at $f = 300$ GHz. Consequently, the NULA is ideal for realizing space-constrained massive MIMO.

⁵One could choose d_g such that both NULA and ULA have the same length and similar spatial resolution. However, this would require an inter-group spacing of multiple wavelengths, which would create grating lobes.

⁶Recall that the spatial resolution is determined by the overall array length [47].

B. How Many BS Antennas Do We Need?

We now focus on the special case of a point-to-point link where a single user is placed at the end-fire direction of the BS, i.e., $(\theta, \phi) = (0^\circ, 0^\circ)$. Therefore, perfect CSI is assumed at the BS. We next seek to find the number of two-element groups that yields the same SNR as a ULA of N antennas. This happens when

$$N_g \mathbf{a}_0^H(0) \text{Re} \{ \bar{\mathbf{Z}}_0 \}^{-1} \mathbf{a}_0(0) = N, \quad (63)$$

which gives

$$N_g = \frac{N(1 - \bar{R}_m^2)}{2(1 - \bar{R}_m \cos(\kappa \bar{d}))}. \quad (64)$$

Since the total number of elements in NULA is $2N_g$, we need $\frac{1 - \bar{R}_m^2}{1 - \bar{R}_m \cos(\kappa \bar{d})}$ antennas compared to a conventional ULA, which is approximately 68% for $\bar{d} = \lambda/5$. As a result, a 32% saving in RF hardware is possible.

TABLE II
MAIN SIMULATION PARAMETERS [20], [35]

Parameter	Value
Carrier frequency	$f = 300$ GHz
Bandwidth	$B = 15$ GHz
BS's input power	$P_t = 20$ dBm
Power per pilot symbol	$P_p = 20$ dBm
Power density of noise	$\sigma^2 = -174$ dBm/Hz
User distance	$r_k \sim \mathcal{U}(5, 15)$ m
Absorption coefficient	$k_{\text{abs}} = 0.0033$ m ⁻¹
Dipole length	$\ell = \lambda/2$
Dipole radius	$\rho = \lambda/500$
Copper conductivity	$\sigma_c = 5.7 \times 10^7$ S/m
Baseband unit	$P_{\text{BB}} = 200$ mW
Phase shifter	$P_{\text{PS}} = 42$ mW
Power amplifier	$P_{\text{PA}} = 60$ mW
DAC	$P_{\text{DAC}} = 110$ mW
Local oscillator	$P_{\text{LO}} = 4$ mW
Mixer	$P_{\text{M}} = 22$ mW

IX. SIMULATION RESULTS

We conduct extensive numerical simulations to assess the performance of the proposed array design. In all experiments, we consider a fractional bandwidth $B/f \leq 0.1$ and LoS links, which yield a spatially narrowband channel.⁷ The other simulation parameters are summarized in Table II. Also, all values in the power consumption model are taken from [20].

⁷In case of beam squint, hybrid beamforming based on true-time-delay could be used [43].

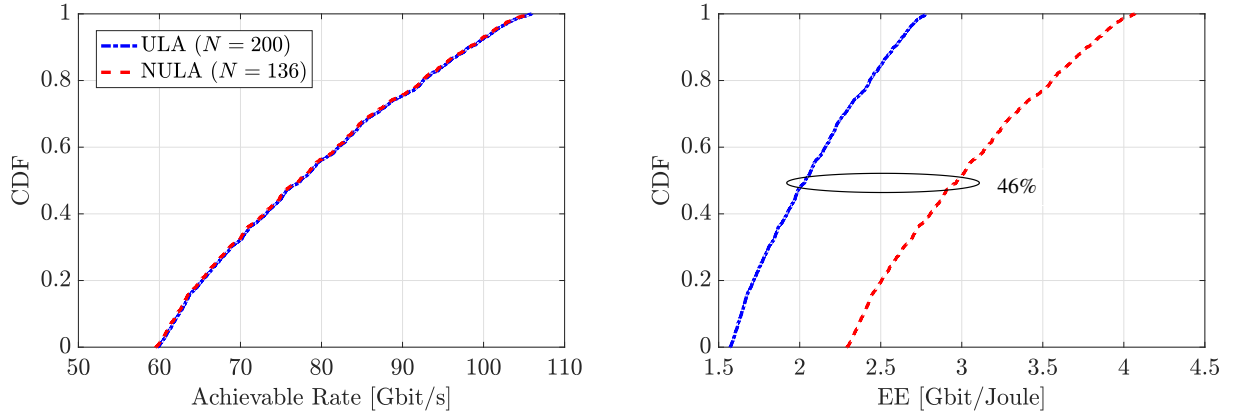


Fig. 7: Results for a point-to-point link. In the NULA, $\bar{N} = 2$, $N_g = 68$, $\bar{d} = \lambda/5$, and $d_g = 1.5\lambda$. In the ULA, $N = 200$ and $d = 1.5\lambda$.

A. Point-to-Point Link

We commence with the simplest case of a point-to-point link. Specifically, a single user is placed at $(\theta, \phi) = (0^\circ, 0^\circ)$. Note that this setup can represent a wireless backhaul link. Due to the fixed user direction, perfect CSI is assumed at the BS. The distance from the BS follows the uniform distribution $\mathcal{U}(5, 15)$ m. The maximum achievable rate and EE are given by $R = B \log_2 \left(1 + \frac{\beta |\mathbf{h}^T \mathbf{w}|^2}{B\sigma^2} \right)$ and R/P_c , respectively. The cumulative distribution function (CDF) of each metric is calculated for 1,000 channel realizations in Fig. 7. As seen, the NULA attains the same achievable rate as ULA, yet with 64 antennas less. This translates roughly to 32% saving in RF circuitry, such as power amplifiers, phase shifters, and combiners, and it comes in perfect agreement with the theoretical result of Section VIII-B. More importantly, the mean EE is improved by 46% compared to a phased array with uniform inter-element spacing.

For the point-to-point deployment, we can employ single-port impedance matching as the beamforming angle is kept fixed. Subsequently, we investigate how this is accomplished. To calculate the active impedance of each dipole, the endfire current vector is decomposed as $\mathbf{i}^* = [\mathbf{i}_0^*, \dots, \mathbf{i}_{N_g-1}^*]^T$, where $\mathbf{i}_{n_g}^* \triangleq [I_{n_g}(0), I_{n_g+1}(0)]^T$ denotes the optimal excitation vector at each antenna pair. This is defined as

$$\mathbf{i}_{n_g}^* = \frac{\sqrt{2P_t} e^{-j\kappa n_g(d_g + \bar{d})}}{\sqrt{N_g \mathbf{a}_0^H(0) \text{Re}\{\mathbf{Z}_0\}^{-1} \mathbf{a}_0(0)}} \text{Re}\{\mathbf{Z}_0\}^{-1} \mathbf{a}_0(0) = \frac{\sqrt{P_t} e^{-j\kappa n_g(d_g + \bar{d})}}{\sqrt{N_g (R_{\text{self}} - R_m \cos(\kappa \bar{d}))}} \begin{bmatrix} R_{\text{self}} - R_m e^{-j\kappa \bar{d}} \\ -R_m + R_{\text{self}} e^{-j\kappa \bar{d}} \end{bmatrix}, \quad (65)$$

where (65) follows from (12) and (45) for $\theta = 0^\circ$. Therefore, for any pair n_g , we have that

$$\frac{I_{n_g+1}(0)}{I_{n_g}(0)} = \frac{-R_m + R_{\text{self}} e^{-j\kappa \bar{d}}}{R_{\text{self}} - R_m e^{-j\kappa \bar{d}}}, \quad (66)$$

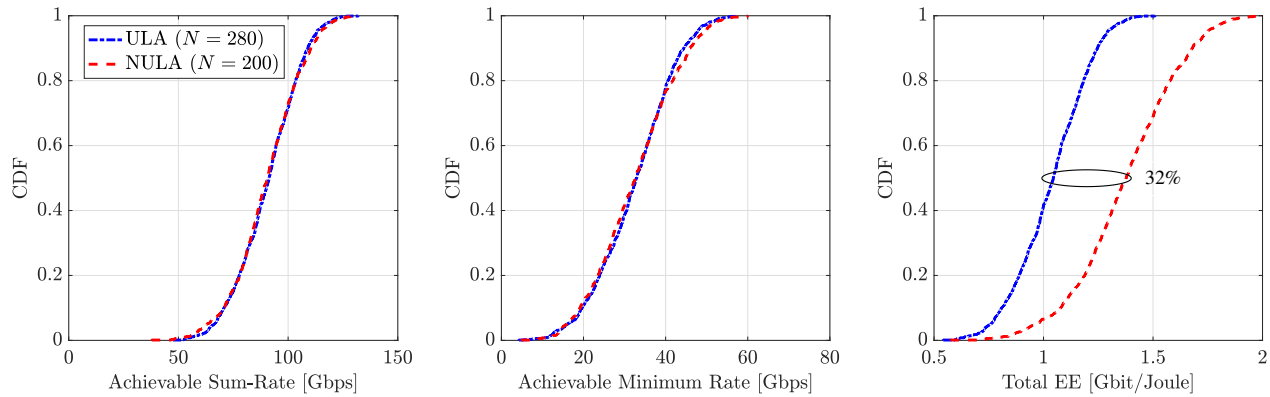


Fig. 8: Results for $K = 2$ users with directions $\theta_k \sim \mathcal{U}(0^\circ, 90^\circ)$ and $\phi_k \sim \mathcal{U}(0^\circ, 360^\circ)$. The BS acquires CSI with partial training of $N_{\text{beam}} = 0.8N$ pilots per user. The dictionary size is $G = N$ for each array design. In the NULA, $\bar{d} = \lambda/5$, and $d_g = 1.5\lambda$. In the ULA, $d = 1.5\lambda$.

which is independent of the group index n_g . Now let

$$\mathbf{Z}_0 \triangleq \begin{bmatrix} Z_{\text{self}} & Z_m \\ Z_m & Z_{\text{self}} \end{bmatrix}, \quad (67)$$

with $\text{Re}\{Z_{\text{self}}\} = R_{\text{self}}$ and $\text{Re}\{Z_m\} = R_m$. The input impedance matrix \mathbf{Z}_0 is computed by the induced EMF method for two side-by-side dipoles [48, Ch. 25]. Since $\mathbf{Z} = \mathbf{I}_{N_g} \otimes \mathbf{Z}_0$, it is straightforward to prove that $\mathbf{Z}_a = \text{blkdiag}(\mathbf{Z}_{0,a}, \dots, \mathbf{Z}_{0,a})$ using the relationship $\mathbf{Z}_a \mathbf{i}^* = \mathbf{Z} \mathbf{i}^*$, where

$$\mathbf{Z}_{0,a} = \begin{bmatrix} Z_{\text{self}} + Z_m \frac{I_{n_g+1}(0)}{I_{n_g}(0)} & 0 \\ 0 & Z_{\text{self}} + Z_m \frac{I_{n_g}(0)}{I_{n_g+1}(0)} \end{bmatrix} = \begin{bmatrix} Z_{\text{self}} + Z_m \frac{-R_m + R_{\text{self}} e^{-j\kappa \bar{d}}}{R_{\text{self}} - R_m e^{-j\kappa \bar{d}}} & 0 \\ 0 & Z_{\text{self}} + Z_m \frac{R_{\text{self}} - R_m e^{-j\kappa \bar{d}}}{-R_m + R_{\text{self}} e^{-j\kappa \bar{d}}} \end{bmatrix}. \quad (68)$$

Consequently, all dipole pairs share a common active impedance matrix whose entries are $[\mathbf{Z}_{0,a}]_{1,1} = 21.84 + j32.89 \Omega$, and $[\mathbf{Z}_{0,a}]_{2,2} = 40.87 + j83.89 \Omega$, for half-wavelength dipoles made of copper and inter-element distance $\bar{d} = \lambda/5$. This is a unique feature of the proposed NULA, as a superdirective ULA would need a different matching impedance for each port because the current amplitude is not uniform along the ports (akin to the source voltages). Thus, the NULA simplifies also single-port matching. Finally, compared to an uncoupled ULA with $Z_{\text{self}} = 75.94 + j41.76 \Omega$, the active impedances $[\mathbf{Z}_{0,a}]_{1,1}$ and $[\mathbf{Z}_{0,a}]_{2,2}$ are not very large, and hence can be easily matched.

B. Multiuser Transmissions with Imperfect CSI

We now consider that the BS simultaneously transmits to K users using MRT. The users' directions are not fixed, and thus the BS acquires the channel estimates $\{\hat{\mathbf{h}}_k\}_{k=1}^K$ through the OMP estimator of

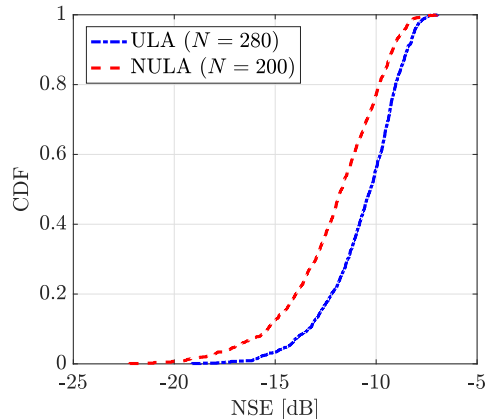


Fig. 9: CDF of NSE for $K = 2$ users and partial beam training.

Section VII-C. Regarding the ULA case, the dictionary is given by $\bar{\mathbf{H}} = [\mathbf{a}(\bar{\theta}_0), \dots, \mathbf{a}(\bar{\theta}_{G-1})]$. The BS treats those estimates as the true channels in the beamforming stage, i.e., $\mathbf{w}_k = \hat{\mathbf{h}}_k^* / \|\hat{\mathbf{h}}_k\|$. The achievable rate of user k is then specified as $R_k = B \log_2(1 + \text{SINR}_k)$, where SINR_k is given by (35). Note that this rate is achieved under the assumption that user k knows $|\mathbf{h}_k^T \mathbf{w}_k|^2$ and $\sum_{i \neq k} |\mathbf{h}_k^T \mathbf{w}_i|^2$ in the decoding stage. These are scalars, and hence are easy to be estimated. For the performance evaluation, the primary metrics are the sum-rate, minimum rate, and total EE defined as $\sum_{k=1}^K R_k$, $\min_k \{R_k\}$, and $\sum_{k=1}^K R_k / P_c$, respectively. Figure 8 shows the results for a two-user transmission. As observed, the NULA boosts the mean EE by 32% as it employs 80 antennas less than the ULA. More remarkably, this improvement comes without compromising the user rates or the angular coverage of the BS, i.e., $\theta_k \sim \mathcal{U}(0^\circ, 90^\circ)$ and $\phi_k \sim \mathcal{U}(0^\circ, 360^\circ)$. Regarding the OMP, a smaller dictionary has been used for the NULA. Nevertheless, this does not introduce significant mismatch errors between the true and discretized AoAs thanks to NULA's wider beamwidth. This is verified by calculating the normalized squared error (NSE) defined as

$$\text{NSE} \triangleq \frac{1}{K} \sum_{k=1}^K \left\| \mathbf{h}_k - \hat{\mathbf{h}}_k \right\|^2 / \|\mathbf{h}_k\|^2. \quad (69)$$

The CDF of this metric is shown in Fig. 9. As observed, the mean error between the actual and estimated channels for NULA is smaller than that of ULA. As a result, the coarse spatial resolution of the NULA provides mismatch robustness, which is crucial to beam alignment and tracking [33].

X. CONCLUSIONS

In this paper, we introduced the novel concept of superdirective dipole pairs. Specifically, we first derived a comprehensive array model that captures the physics of mutual coupling and ohmic losses of nonideal

antennas. Capitalizing on the derived model, we then studied the implementation aspects of superdirectivity, namely the impedance matching and hybrid beamforming problems. To surmount the challenges of superdirective ULAs, we proposed to partition the BS array into multiple two-element groups of sub-wavelength spacing. The resulting NULA simplifies multi-port impedance matching, which is optimal for any beamforming angle. More importantly, it enables the realization of superdirectivity with a single RF chain per beam. Afterwards, we pursued a performance analysis in terms of achievable rate and EE under perfect and imperfect CSI. To this end, approximate closed-form expressions for the signal and multi-user interference powers were provided under MRT. The channel estimation problem was also addressed by employing OMP along with a coupling-aware dictionary. Numerical results were finally provided demonstrating that the proposed method boosts the EE of THz massive MIMO without compromising the data transmission and channel estimation performances. As a result, superdirective NULAs can be a promising approach for realizing low-dimensional massive MIMO with sharp beamforming capabilities. Regarding future work, it would be interesting to consider other types of antennas and array geometries, such as planar and circular arrays.

ACKNOWLEDGEMENTS

This project has received funding from the European Research Council (ERC) under the European Union's Horizon 2020 research and innovation programme (grant agreement No. 101001331).

APPENDIX A

Based on the radiation equations, the electric field is specified as [23, Ch. 3]

$$\mathbf{E}(r, \theta, \phi) = -j\eta \frac{ke^{-j\kappa r}}{4\pi r} (A_\theta \mathbf{e}_\theta + A_\phi \mathbf{e}_\phi), \quad (70)$$

where

$$A_\theta = \int_{-\ell/2}^{\ell/2} I(x') \cos \theta \cos \phi e^{j\kappa x' \cos \phi \sin \theta} \mathbf{d}x = \frac{I(0) \cos \theta \cos \phi}{\sin(\kappa\ell/2)} \int_{-\ell/2}^{\ell/2} \sin(\kappa\ell/2 - \kappa|x'|) e^{j\kappa x' \cos \phi \sin \theta} \mathbf{d}x, \quad (71)$$

and

$$A_\phi = \int_{-\ell/2}^{\ell/2} -I(x') \sin \phi e^{j\kappa x' \cos \phi \sin \theta} \mathbf{d}x = -\frac{I(0) \sin \phi}{\sin(\kappa\ell/2)} \int_{-\ell/2}^{\ell/2} \sin(\kappa\ell/2 - \kappa|x'|) e^{j\kappa x' \cos \phi \sin \theta} \mathbf{d}x. \quad (72)$$

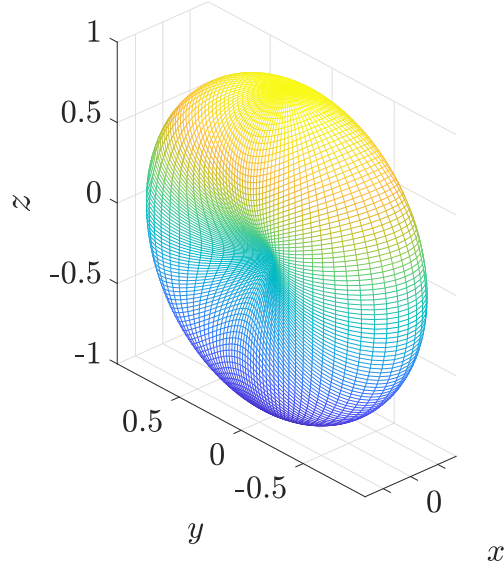


Fig. 10: Squared norm of the vector field pattern $\mathbf{F}(\theta, \phi)$ of a half-wavelength dipole parallel to the x -axis in Cartesian coordinates.

Utilizing the identity [23]

$$\int e^{ax} \sin(\beta x + \gamma) dx = \frac{e^{ax}}{a^2 + \beta^2} [a \sin(\beta x + \gamma) - \beta \cos(\beta x + \gamma)], \quad (73)$$

for $a = j\kappa \cos \phi \sin \theta$, $\beta = \kappa$, and $\gamma = \kappa\ell/2$, and after some algebraic manipulations, we get

$$\int_{-\ell/2}^{\ell/2} \sin(\kappa\ell/2 - \kappa|x'|) e^{j\kappa x' \cos \phi \sin \theta} dx = \frac{2 \cos(\kappa\ell/2 \cos \phi \sin \theta) - \cos(\kappa\ell/2)}{\kappa \sin^2 \phi + \cos^2 \phi \cos^2 \theta}. \quad (74)$$

Combining those equations yields the field expression in (2). The three-dimensional field pattern of a horizontal dipole along the x -axis is depicted in Fig. 10.

APPENDIX B

The inverse matrix of \mathbf{Z}_0 is

$$\text{Re}\{\mathbf{Z}_0\}^{-1} = \frac{1}{R_{\text{self}}^2 - R_m^2} \begin{bmatrix} R_{\text{self}} & -R_m \\ -R_m & R_{\text{self}} \end{bmatrix}. \quad (75)$$

We now need to calculate the square root of the 2×2 matrix $\text{Re}\{\mathbf{Z}_0\}^{-1}$. To do so, we utilize the lemma [49]

$$\mathbf{A}^{1/2} = \frac{1}{t} \begin{bmatrix} a_{11} + s & a_{12} \\ a_{21} & a_{22} + s \end{bmatrix}, \quad (76)$$

for

$$\mathbf{A} = \begin{bmatrix} a_{11} & a_{12} \\ a_{21} & a_{22} \end{bmatrix}, \quad (77)$$

where $s = \sqrt{a_{11}a_{22} - a_{12}a_{21}}$ and $t = \sqrt{a_{11} + a_{22} + 2s}$. In our case, we have that

$$s = \frac{1}{\sqrt{R_{\text{self}}^2 - R_m^2}}, \quad (78)$$

$$t = \sqrt{\frac{2R_{\text{self}} + 2\sqrt{R_{\text{self}}^2 - R_m^2}}{R_{\text{self}}^2 - R_m^2}}. \quad (79)$$

Applying (76) to $\text{Re}\{\mathbf{Z}_0\}^{-1}$, and after basic algebra, yields

$$\text{Re}\{\mathbf{Z}_0\}^{-1/2} = \frac{1}{\sqrt{2R_{\text{self}} + 2\sqrt{R_{\text{self}}^2 - R_m^2}}} \begin{bmatrix} \frac{R_{\text{self}}}{\sqrt{R_{\text{self}}^2 - R_m^2}} + 1 & -\frac{R_m}{\sqrt{R_{\text{self}}^2 - R_m^2}} \\ -\frac{R_m}{\sqrt{R_{\text{self}}^2 - R_m^2}} & \frac{R_{\text{self}}}{\sqrt{R_{\text{self}}^2 - R_m^2}} + 1 \end{bmatrix}, \quad (80)$$

and

$$\text{Re}\{\mathbf{Z}_0\}^{-1/2} \mathbf{a}_0(\theta) = \frac{1}{\sqrt{2R_{\text{self}} + 2\sqrt{R_{\text{self}}^2 - R_m^2}}} \begin{bmatrix} \frac{R_{\text{self}}}{\sqrt{R_{\text{self}}^2 - R_m^2}} + 1 - \frac{R_m}{\sqrt{R_{\text{self}}^2 - R_m^2}} e^{-j\kappa\bar{d}\cos\theta} \\ -\frac{R_m}{\sqrt{R_{\text{self}}^2 - R_m^2}} + \left(\frac{R_{\text{self}}}{\sqrt{R_{\text{self}}^2 - R_m^2}} + 1\right) e^{-j\kappa\bar{d}\cos\theta} \end{bmatrix}. \quad (81)$$

Lastly, calculating the magnitudes of the entries of $\text{Re}\{\mathbf{Z}_0\}^{-1/2} \mathbf{a}_0(\theta)$, and some algebraic manipulations, we obtain (31).

APPENDIX C

Because $\mathbf{Z} \approx \mathbf{I}_{N_g} \otimes \mathbf{Z}_0$ in the proposed NULA, (18) becomes

$$\mathbf{Z}_M = \begin{bmatrix} -j\text{Im}\{Z_s\}\mathbf{I}_{N_g} \otimes \mathbf{I}_2 & -j\sqrt{R_s}\mathbf{I}_{N_g} \otimes \text{Re}\{\mathbf{Z}_0\}^{1/2} \\ -j\sqrt{R_s}\mathbf{I}_{N_g} \otimes \text{Re}\{\mathbf{Z}_0\}^{1/2} & -j\mathbf{I}_{N_g} \otimes \text{Im}\{\mathbf{Z}_0\} \end{bmatrix}. \quad (82)$$

We now partition the vectors of voltages and currents at the input and output of the impedance matching network as $\mathbf{v}_M = [\mathbf{v}_{M,0}, \dots, \mathbf{v}_{M,N_g-1}]^T$, $\mathbf{i}_M = [\mathbf{i}_{M,0}, \dots, \mathbf{i}_{M,N_g-1}]^T$, $\mathbf{v} = [\mathbf{v}_0, \dots, \mathbf{v}_{N_g-1}]^T$, and $\mathbf{i} = [\mathbf{i}_0, \dots, \mathbf{i}_{N_g-1}]^T$, where $\mathbf{v}_{M,n_g} = [v_{M,n_g}, v_{M,n_g+1}]^T$ is the vector of voltages at the n_g th input port pair; \mathbf{i}_{M,n_g} , \mathbf{v}_{n_g} , and \mathbf{i}_{n_g} are defined similarly. By using (82) and the previous decompositions, (16) is

recast as

$$\begin{bmatrix} \begin{bmatrix} \mathbf{v}_{M,0} \\ \mathbf{v}_0 \end{bmatrix} \\ \vdots \\ \begin{bmatrix} \mathbf{v}_{M,N_g-1} \\ \mathbf{v}_{N_g-1} \end{bmatrix} \end{bmatrix} = \begin{bmatrix} \mathbf{Z}_{M,0} \begin{bmatrix} \mathbf{i}_{M,0} \\ -\mathbf{i}_0 \end{bmatrix} \\ \vdots \\ \mathbf{Z}_{M,0} \begin{bmatrix} \mathbf{i}_{M,N_g-1} \\ -\mathbf{i}_{N_g-1} \end{bmatrix} \end{bmatrix}, \quad (83)$$

which shows that \mathbf{Z}_M comprises N_g four-port matching networks, which are independent of each other.

APPENDIX D

We have that

$$\begin{aligned} \frac{|\mathbf{a}^H(\theta_k) \text{Re} \{ \bar{\mathbf{Z}}_{\text{approx}} \}^{-1} \mathbf{a}(\theta_i)|^2}{\mathbf{a}^H(\theta_i) \text{Re} \{ \bar{\mathbf{Z}}_{\text{approx}} \}^{-1} \mathbf{a}(\theta_i)} &= \frac{|(\mathbf{a}_g^H(\theta_k) \otimes \mathbf{a}_0^H(\theta_k)) (\mathbf{I}_{N_g} \otimes \text{Re} \{ \bar{\mathbf{Z}}_0 \}^{-1}) (\mathbf{a}_g(\theta_i) \otimes \mathbf{a}_0(\theta_i))|^2}{(\mathbf{a}_g^H(\theta_i) \otimes \mathbf{a}_0^H(\theta_i)) (\mathbf{I}_{N_g} \otimes \text{Re} \{ \bar{\mathbf{Z}}_0 \}^{-1}) (\mathbf{a}_g(\theta_i) \otimes \mathbf{a}_0(\theta_i))} \\ &= \frac{|\mathbf{a}_0^H(\theta_k) \text{Re} \{ \bar{\mathbf{Z}}_0 \}^{-1} \mathbf{a}_0(\theta_i)|^2}{\mathbf{a}_0^H(\theta_i) \text{Re} \{ \bar{\mathbf{Z}}_0 \}^{-1} \mathbf{a}_0(\theta_i)} \frac{|\mathbf{a}_g^H(\theta_k) \mathbf{a}_g(\theta_i)|^2}{N_g}, \end{aligned} \quad (84)$$

where the identity $(\mathbf{A} \otimes \mathbf{B})(\mathbf{C} \otimes \mathbf{D}) = (\mathbf{AC}) \otimes (\mathbf{BD})$ has been applied twice. Lastly,

$$\begin{aligned} \frac{|\mathbf{a}_g^H(\theta_k) \mathbf{a}_g(\theta_i)|^2}{N_g} &= \frac{1}{N_g} \left| \sum_{n_g=0}^{N_g-1} e^{-j\kappa n_g (d_g + (\bar{N}-1)\bar{d}) (\cos \theta_k - \cos \theta_i)} \right|^2 \\ &= \frac{1}{N_g} \left| \frac{1 - e^{-j\kappa N_g (d_g + (\bar{N}-1)\bar{d}) (\cos \theta_k - \cos \theta_i)}}{1 - e^{-j\kappa (d_g + (\bar{N}-1)\bar{d}) (\cos \theta_k - \cos \theta_i)}} \right|^2 \end{aligned} \quad (85)$$

$$= N_g |D_{N_g} (\kappa (d_g + (\bar{N}-1)\bar{d}) (\cos \theta_k - \cos \theta_i))|^2, \quad (86)$$

which completes the proof.

REFERENCES

- [1] T. Kashima *et al.*, "Large scale massive MIMO field trial for 5G mobile communications system," in *Proc. IEEE ISAP*, Oct. 2016, pp. 602-603.
- [2] W. Roh *et al.*, "Millimeter-wave beamforming as an enabling technology for 5G cellular communications: Theoretical feasibility and prototype results," *IEEE Commun. Mag.*, vol. 52, no. 2, pp. 106-113, Feb. 2014.
- [3] M. Xiao *et al.*, "Millimeter wave communications for future mobile networks," *IEEE J. Sel. Areas Commun.*, vol. 35, no. 9, pp. 1909-1935, Sept. 2017.
- [4] T. S. Rappaport *et al.*, "Wireless communications and applications above 100 GHz: Opportunities and challenges for 6G and beyond," *IEEE Access*, vol. 7, pp. 78729-78757, 2019.

- [5] M. Matthaiou *et al.*, “The road to 6G: Ten physical layer challenges for communications engineers,” *IEEE Commun. Mag.*, vol. 59, no. 1, pp. 64-69, Jan. 2021.
- [6] I. F. Akyildiz, C. Han, and S. Nie, “Combating the distance problem in the millimeter wave and terahertz frequency bands,” *IEEE Commun. Mag.*, vol. 56, no. 6, pp. 102-108, Jun. 2018.
- [7] J. Zhang *et al.*, “Prospective multiple antenna technologies for beyond 5G,” *IEEE J. Sel. Areas Commun.*, vol. 38, no. 8, pp. 1637–1660, Aug. 2020.
- [8] H. J. Song and N. Lee, “Terahertz communications: Challenges in the next decade,” *IEEE Trans. THz Sci. Technol.*, vol. 12, no. 2, pp. 105-117, Mar. 2022.
- [9] E. Björnson, L. Sanguinetti, J. Hoydis, and M. Debbah, “Optimal design of energy-efficient multi-user MIMO systems: Is massive MIMO the answer?,” *IEEE Trans. Wireless Commun.*, vol. 14, no. 6, pp. 3059-3075, Jun. 2015.
- [10] O. E. Ayach, R. W. Heath, Jr., S. Abu-Surra, S. Rajagopal, and Z. Pi, “The capacity optimality of beam steering in large millimeter wave MIMO systems,” in *Proc. IEEE SPAWC*, Jun. 2012, pp. 100–104.
- [11] A. Uzkov, “An approach to the problem of optimum directive antenna design,” *Comptes Rendus (Doklady) de l’Academie des Sci. de l’URSS*, vol. 53, no. 1, pp. 35–38, 1946.
- [12] M. L. Morris *et al.*, “Superdirectivity in MIMO systems,” *IEEE Trans. Antennas Propag.*, vol. 53, no. 9, pp. 2850-2857, Sept. 2005.
- [13] N. W. Bikhazi and M. A. Jensen, “The relationship between antenna loss and superdirectivity in MIMO systems,” *IEEE Trans. Wireless Commun.*, vol. 6, no. 5, pp. 1796-1802, May 2007.
- [14] R. J. Williams, E. de Carvalho, and T. L. Marzetta, “A communication model for large intelligent surfaces,” in *Proc. IEEE ICC*, Jun. 2020.
- [15] A. S. Y. Poon and D. N. C. Tse, “Does superdirectivity increase the degrees of freedom in wireless channels?,” in *Proc. IEEE ISIT*, Jun. 2015, pp. 1232-1236.
- [16] A. Haskou, A. Sharaiha, and S. Collardey, “Design of small parasitic loaded superdirective end-fire antenna arrays,” *IEEE Trans. Antennas Propag.*, vol. 63, no. 12, pp. 5456-5464, Dec. 2015.
- [17] T. Lonsky, J. Kracek, and P. Hazdra, “Superdirective linear dipole array optimization,” *IEEE Antennas Wireless Propag. Lett.*, vol. 19, no. 6, pp. 902-906, Jun. 2020.
- [18] C. Lin and G. Y. L. Li, “Terahertz communications: An array-of-subarrays solution,” *IEEE Commun. Mag.*, vol. 54, no. 12, pp. 124-131, Dec. 2016.
- [19] H. Li, M. Li, and Q. Liu, “Hybrid beamforming with dynamic subarrays and low-resolution PSs for mmWave MU-MISO systems,” *IEEE Trans. Commun.*, vol. 68, no. 1, pp. 602-614, Jan. 2020.
- [20] L. Yan, C. Han, and J. Yuan, “A dynamic array-of-subarrays architecture and hybrid precoding algorithms for terahertz wireless communications,” *IEEE J. Sel. Areas Commun.*, vol. 38, no. 9, pp. 2041-2056, Sept. 2020.
- [21] K. Dovelos, S. D. Assimonis, H. Q. Ngo, B. Bellalta, and M. Matthaiou, “Intelligent reflecting surfaces at terahertz bands: Channel modeling and analysis,” in *Proc. IEEE ICC*, Jun. 2021, pp. 1-6.
- [22] R. Goossens and H. Rogier, “Optimal beamforming in the presence of mutual coupling,” in *Proc. IEEE SCVT*, Nov. 2006, pp. 13-18.
- [23] C. A. Balanis, *Antenna Theory: Analysis and Design*, 3rd ed., John Wiley & Sons, 2012.
- [24] M. T. Ivrlač and J. A. Nосsek, “High-efficiency super-gain antenna arrays,” in *Proc. Int. ITG WSA*, Feb. 2010, pp. 369-374.
- [25] Y. Fei, Y. Fan, B. K. Lau, and J. S. Thompson, “Optimal single-port matching impedance for capacity maximization in compact MIMO arrays,” *IEEE Trans. Antennas Propag.*, vol. 56, no. 11, pp. 3566-3575, Nov. 2008.
- [26] M. T. Ivrlač and J. A. Nосsek, “Toward a circuit theory of communication,” *IEEE Trans. Circuits Syst.*, vol. 57, no. 7, pp. 1663-1683, Jul. 2010.

- [27] D. M. Pozar, *Microwave Engineering*, John Wiley & Sons, 2009.
- [28] M. T. Ivrlač and J. A. Nossek, “The multiport communication theory,” *IEEE Circuits Syst. Mag.*, vol. 14, no. 3, pp. 27-44, Aug. 2014.
- [29] S. Shen and R. D. Murch, “Impedance matching for compact multiple antenna systems in random RF fields,” *IEEE Trans. Antennas Propag.*, vol. 64, no. 2, pp. 820-825, Feb. 2016.
- [30] T. Laas, J. A. Nossek, and W. Xu, “Limits of transmit and receive array gain in massive MIMO,” in *Proc. IEEE WCNC*, May 2020.
- [31] S. D. Assimonis, T. V. Yioultsis, and C. S. Antonopoulos, “Design and optimization of uniplanar EBG structures for low profile antenna applications and mutual coupling reduction,” *IEEE Trans. Antennas Propag.*, vol. 60, no. 10, pp. 4944-4949, Oct. 2012.
- [32] X. Yang *et al.*, “Hardware-constrained millimeter-wave systems for 5G: Challenges, opportunities, and solutions,” *IEEE Commun. Mag.*, vol. 57, no. 1, pp. 44-50, Jan. 2019.
- [33] X. Gao *et al.*, “Fast channel tracking for terahertz beamspace massive MIMO systems,” *IEEE Trans. Veh. Technol.*, vol. 66, no. 7, pp. 5689-5696, Jul. 2017.
- [34] C. Lin and G. Y. Li, “Indoor terahertz communications: How many antenna arrays are needed?,” *IEEE Trans. Wireless Commun.*, vol. 14, no. 6, pp. 3097-3107, Jun. 2015.
- [35] C. Han, A. O. Bicen, and I. F. Akyildiz, “Multi-ray channel modeling and wideband characterization for wireless communications in the terahertz band,” *IEEE Trans. Wireless Commun.*, vol. 14, no. 5, pp. 2402-2412, May 2015.
- [36] L. N. Ribeiro, S. Schwarz, M. Rupp, and A. L. F. de Almeida, “Energy efficiency of mmWave massive MIMO precoding with low-resolution DACs,” *IEEE J. Sel. Topics Signal Process.*, vol. 12, no. 2, pp. 298-312, May 2018.
- [37] E. Björnson, J. Hoydis, and L. Sanguinetti, *Massive MIMO Networks: Spectral, Energy, and Hardware Efficiency*, Foundations and Trends in Signal Processing: vol. 11, no. 3-4, pp. 154-655, 2017.
- [38] M. T. Ivrlač and J. A. Nossek, “Physical modeling of communication systems in information theory,” in *Proc. IEEE ISIT*, Jul. 2009, pp. 2179-2183.
- [39] M. Jensen and J. Wallace, “A review of antennas and propagation for MIMO wireless communications,” *IEEE Trans. Antennas Propag.*, vol. 52, no. 11, pp. 2810-2824, Nov. 2004.
- [40] C. Hermosilla, R. Feick, R. A. Valenzuela, and L. Ahumada, “Improving MIMO capacity with directive antennas for outdoor-indoor scenarios,” in *Proc. IEEE VTC*, May 2008, pp. 414-41.
- [41] T. L. Marzetta, E. G. Larsson, H. Yang, and H. Q. Ngo, *Fundamentals of Massive MIMO*. Cambridge, U.K.: Cambridge Univ. Press, 2016.
- [42] T. Laas, J. A. Nossek, S. Bazzi and W. Xu, “On reciprocity in physically consistent TDD systems with coupled antennas,” *IEEE Trans. Wireless Commun.*, vol. 19, no. 10, pp. 6440-6453, Oct. 2020.
- [43] K. Dovelos, M. Matthaiou, H. Q. Ngo, and B. Bellalta, “Channel estimation and hybrid combining for wideband terahertz massive MIMO systems,” *IEEE J. Sel. Areas Commun.*, vol. 39, no. 6, pp. 1604-1620, Jun. 2021.
- [44] J. Lee, G.-T. Gil, and Y. H. Lee, “Exploiting spatial sparsity for estimating channels of hybrid MIMO systems in millimeter wave communications,” in *Proc. IEEE GLOBECOM*, Dec. 2014, pp. 3326-3331.
- [45] O. E. Ayach, S. Rajagopal, S. Abu-Surra, Z. Pi, and R. W. Heath, Jr., “Spatially sparse precoding in millimeter wave MIMO systems,” *IEEE Trans. Wireless Commun.*, vol. 13, no. 3, pp. 1499-1513, Mar. 2014.
- [46] J. A. Tropp and A. C. Gilbert, “Signal recovery from random measurements via orthogonal matching pursuit,” *IEEE Trans. Inf. Theory*, vol. 53, no. 12, pp. 4655-4666, Dec. 2007.
- [47] D. Tse and P. Viswanath, *Fundamentals of Wireless Communication*, New York, USA: Cambridge Univ. Press, 2005.
- [48] S. J. Orfanidis, *Electromagnetic Waves and Antennas*, Rutgers University, 2016.
- [49] B. W. Levinger, “The square root of a 2×2 matrix,” *Mathematics Mag.*, vol. 53, no. 4, pp. 222-224, 1980.